

Pseudopotential Formalism for Fractional Chern Insulators

Ching Hua Lee¹, Ronny Thomale^{2,3}, and Xiao-Liang Qi¹

¹*Department of Physics, Stanford University, Stanford, CA 94305, USA*

²*Institut de théorie des phénomènes physiques, École Polytechnique Fédérale de Lausanne (EPFL), CH-1015 Lausanne and*

³*Institute for Theoretical Physics and Astrophysics, University of Würzburg, D 97074 Würzburg*

(Dated: November 1, 2018)

Recently, generalizations of fractional quantum Hall (FQH) states known as fractional quantum anomalous Hall or, equivalently, fractional Chern insulators states have been realized in lattice models. Ideal wavefunctions such as the Laughlin wavefunction, as well as their corresponding trial Hamiltonians, have been vital to characterizing FQH phases. The Wannier function representation of fractional Chern insulators proposed in [X.-L. Qi, Phys. Rev. Lett. **107**, 126803] defines an approach to generalize these concepts to fractional Chern insulators. In this paper, we apply the Wannier function representation to develop a systematic pseudopotential formalism for fractional Chern insulators. The family of pseudopotential Hamiltonians is defined as the set of projectors onto asymptotic relative angular momentum components which forms an orthogonal basis of two-body Hamiltonians with magnetic translation symmetry. This approach serves both as an expansion tool for interactions and as a definition of positive semidefinite Hamiltonians for which the ideal fractional Chern insulator wavefunctions are exact nullspace modes. We compare the short-range two-body pseudopotential expansion of various fractional Chern insulator models at filling $\mu = 1/3$ in phase regimes where a Laughlin-type ground state is expected to be realized. We also discuss the effect of inhomogeneous Berry curvature which leads to components of the Hamiltonian that cannot be expanded into pseudopotentials, and elaborate on their role in determining low energy theories for fractional Chern insulators. Finally, we generalize our Chern pseudopotential approach to interactions involving more than two bodies with the goal of facilitating the identification of non-Abelian fractional Chern insulators.

I. INTRODUCTION

The field of topological insulators (TIs) is currently witnessing enormous interest in condensed matter¹⁻³. The predecessor of TIs is the integer quantum Hall effect (IQHE)⁴ realized in a two-dimensional electron gas with a strong perpendicular magnetic field. Similar to other TIs discovered more recently, the IQHE is a gapped state of matter characterized by topologically robust edge states and a bulk topological invariant known as the Chern number or the Thouless-Kohmoto-Nightingale-den Nijs (TKNN) number⁵. The IQH state has been generalized to lattice models without orbital magnetic field⁶, which are named as quantum anomalous Hall (QAH) states or Chern insulators (CI). QAH states have been proposed in realistic materials⁷⁻⁹. In 1983, the fractional quantum Hall effect (FQHE) was discovered in systems with a fractionally filled Landau level^{10,11}. Since then, the FQHE has become a paradigmatic example of a topologically ordered phase¹² where interactions exhibit non-perturbative roles. Numerous fundamental developments evolved out of this direction, such as the concept of non-Abelian statistics which forms the foundation of topological quantum computation^{13,14}. One fundamental difference from IQHE is that the flatness of the Landau level and its associated freezing of kinetic energy appear to be necessary conditions for the FQHE state to be energetically preferable.

This immediately provokes the question of whether a fractional Chern insulator (FCI) can be realized, i.e. a lattice version of the FQHE without an external magnetic field. Taking a CI such as Haldane's honeycomb

model⁶ as a natural starting point, the task then is to drive the system into the flat band limit where the chemical potential lies within this band, e.g. at fractional one third filling, which is well separated from the other bands and hence accomplishes a FQHE-type lattice scenario. (Unlike the quantum Hall case, the FCI filling is not given by the ratio of electrons over magnetic flux quanta, but the chemical potential of the lattice model.) Different groups have recently independently pursued this direction, proposing FCI models on the honeycomb, kagome, square, and checkerboard lattice¹⁵⁻¹⁷. In different ways, the flattening of the Chern band can be accomplished through geometric frustration (e.g. long-range hopping)^{15,16}, multi-band effects¹⁷, and multi-orbital character¹⁸. While the s and p -type orbitals in previous candidates materials for topological insulators would assume only moderate interactions from small hybridizations, d -orbital-type systems provide an arena for both strong correlations and topological band structures¹⁹. First numerical investigations of the FCI phases on a torus at one third band filling found indications of a three-fold topologically degenerate ground state separated from the other energy levels by a gap, where the flux insertion showed level crossings with no level repulsion between them, and the Chern numbers of these many-body ground states found to be $1/3$ each^{16,20}. While this already gives a strong hint that a Laughlin-type fractional Chern phase might be realized, this does not yet completely rule out a competing charge density wave (CDW) state at this filling, which can show similar fractional Chern numbers in the ground states, level degeneracy, and a gap. Further evidence against a CDW

state, however, has been found by finite size scaling, entanglement measures, and the distribution of ground state momenta as a function of cluster size²¹. Compared to the FQHE for which the joint perspective of energy and entanglement measures generally gives a consistent and complementary picture, the current stage of FCI models particularly calls for further investigation.

In this paper, we focus on further developing the understanding of FCI phases from the perspective of energetics and interactions. In general, FCIs involve different scales such as the kinetic bandwidth of the fractionally filled Chern band, the gap separation from other bands, as well as the magnitude and range of interactions. Even if we assume a conventional FQHE-type parameter window where inter-band scattering is neglected and the bandwidth of the fractional Chern band is assumed small versus the interaction strength, a crucial complication of FCI models is the inhomogeneous Berry curvature which has no quantum Hall analogue. As a signature of this difference, the Platzman-Girvin-MacDonald algebra²² of the lowest Landau level (LLL) can only be mapped to the lattice Chern density operators in the continuum limit as well as for homogeneous Berry curvature²³, from where Hamiltonian theories can be constructed²⁴. However, an exact one-to-one mapping between FQH and FCI states with Chern number $C = 1$ has been established by the Wannier state representation of Chern insulators²⁵ despite of the inhomogeneous Berry curvature. (One-dimensional) Wannier states are single particle states which are localized in real space in one spatial direction (such as x), but are momentum eigenstates in the orthogonal direction y . Different Wannier states are related by translation in x direction, and all Wannier states form a complete basis of the single particle Hilbert space defined by a non-degenerate energy band. The exact mapping between FQH and FCI is obtained by mapping Landau level wavefunctions in the Landau gauge to the Wannier states in FCI. More details of this mapping will be reviewed in Sec. II. From the Wannier state representation, we learn that the effect of inhomogeneous Berry curvature is absent if we consider a special Hamiltonian obtained by mapping a FQH Hamiltonian to the FCI system. In other words, the effect of inhomogeneous Berry curvature in an FCI strongly depends on the interaction Hamiltonian. In two recent works^{26,27}, the Wannier state representation and its further improvement has been investigated in both fermionic and bosonic FCI systems. In the bosonic $\nu = 1/2$ FCI, the wavefunction proposed by the Wannier state representation has a high overlap with the exact ground state wavefunction obtained by exact diagonalization²⁷. In the fermionic $\nu = 1/3$ case, such a high overlap is also achieved given that the Wannier states are modified²⁶. Therefore the validity of the Wannier state representation has been demonstrated at least in those simplest FCI states.

An important part of this paper will concern the development of a pseudopotential (PP) formalism for fractional Chern insulators. Previously, PPs have been estab-

lished in the context of FQHE²⁸. PPs are partial wave expansions of the Coulomb interactions. The resulting expansion quantum number is the relative angular momentum m of two particles (with m even for bosons and odd for fermions) where the expansion coefficients V_m denote the energy penalty of two particles having a relative angular momentum of m . In the same way the Landau level wave functions were used as a basis for defining such an expansion in FQHE, we now employ a similar construction for the FCI Wannier functions²⁵. PPs proved extremely useful in FQHE not only to give a universal classification of different interaction profiles, but also to obtain an adequate description of general FQHE phase diagrams. Furthermore, many paradigmatic FQH wave functions are exact ground states of certain PP Hamiltonians for which representative finite size studies would be more accurate to resolve their universal properties than for a generic interaction scenario²⁹⁻³¹. In adapting this concept to FCI models, we can hope for a similarly promising route to a deeper and more universal understanding of FCI Hamiltonians.

The paper is organized as follows. In Section II, we review and expand the description of the Wannier state representation of fractional Chern bands. This lays the foundation for the definition of FCI PPs, for which we first review the PP formalism for FQHE and subsequently develop the FCI formulation of PPs in Section III. In Section IV, we apply our PP formalism to different FCI models and their interaction profiles. We find that, as a direct consequence of inhomogeneous Berry curvature, there is a portion of the interactions which cannot be expanded in PPs. These observations will be analysed in detail in Section V. There, we classify what type of center-of-mass (CM) breaking and magnetic-translation-group (MT) breaking scattering elements appear in FCI interactions, and how these symmetries are potentially reemergent in an effective low energy theory of the problem^{32,33}. In Section VI, we generalize the FCI PP principle to many-body interactions, which enables us to define exact Hamiltonians for non-Abelian FCI phases. In Section VII, we conclude that the pseudopotential formalism establishes a suitable platform to further investigate and analyze new states of matter in FCIs.

II. WANNIER STATE REPRESENTATION OF FRACTIONAL CHERN BANDS

In this section, we review the Wannier state representation of FCIs proposed in Ref. 25. The idea of this approach is to find a suitable single-particle basis, the one-dimensional (1D) Wannier state basis, and to use this basis to establish an exact mapping between FCI and FQH states. While a cylindrical geometry was employed in Ref. 25, the discussion can also be formulated on the torus geometry³⁴ which we use in the following. (The torus formulation of the Wannier state representation has

also been investigated independently in Ref.^{26,27}.)

Consider a band insulator with the Hamiltonian

$$H = \sum_{i,j,\alpha,\beta} c_{i\alpha}^\dagger h_{ij}^{\alpha\beta} c_{j\beta}, \quad (1)$$

with i, j being the site indices of a two-dimensional lattice with periodic boundary conditions and $\alpha, \beta = 1, 2, \dots, N$ labeling internal states in each unit cell such as orbital and spin states. With translation symmetry $h_{ij}^{\alpha\beta} = h_{\mathbf{r}_j - \mathbf{r}_i}^{\alpha\beta}$, the Hamiltonian can be written in momentum space as

$$H = \sum_{\mathbf{k}} c_{\mathbf{k}\alpha}^\dagger h_{\mathbf{k}}^{\alpha\beta} c_{\mathbf{k}\beta}, \quad (2)$$

with

$$c_{\mathbf{k}\alpha} = \frac{1}{\sqrt{L_x L_y}} \sum_i c_{i\alpha} e^{-i\mathbf{k}\cdot\mathbf{r}_i},$$

$$h_{\mathbf{r}_j - \mathbf{r}_i}^{\alpha\beta} = \frac{1}{L_x L_y} \sum_{\mathbf{k}} h_{\mathbf{k}}^{\alpha\beta} e^{-i\mathbf{k}\cdot(\mathbf{r}_j - \mathbf{r}_i)}.$$

We use L_x, L_y to denote the number of lattice sites in x and y direction, respectively. The momentum \mathbf{k} takes values of $\left(\frac{2\pi n_x}{L_x}, \frac{2\pi n_y}{L_y}\right)$, with $n_x = 1, 2, \dots, L_x$, $n_y = 1, 2, \dots, L_y$ integers. The Hamiltonian matrix $h_{\mathbf{k}}$ can be diagonalized to obtain the eigenstates

$$h_{\mathbf{k}} |n, \mathbf{k}\rangle = E_{n\mathbf{k}} |n, \mathbf{k}\rangle, \quad n = 1, 2, \dots, N. \quad (3)$$

We are interested in the system with a lowest energy band $E_{1\mathbf{k}}$ occupied, and a gap separating this band from all other bands. Since only the lowest band will be involved, we will denote $|1, \mathbf{k}\rangle$ by $|\mathbf{k}\rangle$ for simplicity.

In the thermodynamic limit $L_x, L_y \rightarrow \infty$, \mathbf{k} is a good quantum number and the Berry's phase gauge field $\mathbf{a} = -i \langle \mathbf{k} | \nabla_{\mathbf{k}} | \mathbf{k} \rangle$ can be defined, which determines the first Chern number as the flux of the gauge field in the Brillouin zone: $C_1 = \frac{1}{2\pi} \int_{BZ} d^2\mathbf{k} \nabla \times \mathbf{a}$. For the realization of FCIs, we are interested in a band with $C_1 \neq 0$. More specifically, in this paper we will focus on $C_1 = 1$ systems. Moreover, for finite L_x, L_y , it is necessary to generalize the definition of a Berry's phase gauge field and Chern number to the case of $|\mathbf{k}\rangle$ with a discrete \mathbf{k} variable.

We start from the definition of 1D Wannier states

$$|W_{nk_y}\rangle = \frac{1}{\sqrt{L_x}} \sum_{k_x} e^{-ik_x n} e^{i\varphi_{\mathbf{k}}} |\mathbf{k}\rangle, \quad (4)$$

which is a Fourier transform of $|\mathbf{k}\rangle$ in the x -direction, but which remains an eigenstate of k_y . Since the state $|\mathbf{k}\rangle$ is only determined by the Hamiltonian up to a phase, the phase factor $e^{i\varphi_{\mathbf{k}}}$ is not pre-determined. As was discussed in Refs. 25 and 35, the phase ambiguity can be fixed by defining the projected position operator $\hat{x} = P x P$ with $P = \sum_{\mathbf{k}} |\mathbf{k}\rangle \langle \mathbf{k}|$, the projection operator to the occupied band, and $x = \sum_{i,\alpha} x_i |i, \alpha\rangle \langle i, \alpha|$ the position operator. However, in a system with periodic boundary conditions

in x -direction, it will be slightly more problematic to apply this definition of x due to the dependence on the choice of the boundary site. As pointed out in Ref. 34, this problem can be resolved by defining a unitary operator

$$X = \exp \left[i x \frac{2\pi}{L_x} \right] = \exp \left[i \sum_i \frac{2\pi x_i}{L_x} \sum_{\alpha} |i\alpha\rangle \langle i\alpha| \right]. \quad (5)$$

This definition preserves the periodicity $x \rightarrow x + L_x$. The eigenstates of this operator are the states localized on a given site n in x -direction. We define the projected operator

$$\hat{X} = P X P. \quad (6)$$

In momentum space, $\langle \mathbf{k} | \hat{X} | \mathbf{k}' \rangle = \langle \mathbf{k} | X | \mathbf{k}' \rangle$. It is easy to see that X shifts the momentum k_x by $2\pi/L_x$, since

$$|\mathbf{k}\rangle = \frac{1}{\sqrt{L_x L_y}} \sum_{i,\alpha} u_{\mathbf{k}\alpha} e^{ix_i k_i} |i, \alpha\rangle,$$

$$X |\mathbf{k}\rangle = \sum_{i,\alpha} u_{\mathbf{k}\alpha} e^{ix_i (k_x + \frac{2\pi}{L_x})} |i, \alpha\rangle, \quad (7)$$

with $u_{\mathbf{k}\alpha} = \sqrt{L_x L_y} \langle 0, \alpha | \mathbf{k} \rangle$ the periodic part of the Bloch wave function. Therefore, the only nonzero matrix element of $\langle \mathbf{k} | X | \mathbf{k}' \rangle$ is

$$F_{k_x k_y} \equiv \langle k_x + 2\pi/L_x, k_y | X | k_x, k_y \rangle$$

$$= \sum_{\alpha} u_{k_x + \frac{2\pi}{L_x}, k_y, \alpha}^* u_{k_x, k_y, \alpha}. \quad (8)$$

In the subspace of states with given k_y , the matrix of \hat{X} in momentum representation is

$$\hat{X} = \begin{pmatrix} 0 & \dots & F_{2\pi} \\ F_{2\pi/L_x} & 0 & \dots \\ \dots & F_{4\pi/L_x} & \dots \\ \dots & \dots & \dots \\ \dots & \dots & F_{(L_x-1)\pi/L_x} & 0 \end{pmatrix}, \quad (9)$$

where the omitted index k_y is the same for all states.

In the thermodynamic limit $L_x \rightarrow \infty$, $F_{k_x k_y} \simeq 1 - i \frac{2\pi}{L_x} a_x(\mathbf{k})$, with a_x the x component of the Berry's phase gauge field. For finite L_x , $|F_{k_x k_y}|$ should be close to but not exactly equal to 1. Therefore, \hat{X} is an approximately unitary matrix. To define the maximally localized Wannier states, we deform the \hat{X} operator to a unitary operator by defining

$$F_{k_x k_y} = |F_{k_x k_y}| e^{-iA_{k_x k_y}}$$

$$\bar{X} = \begin{pmatrix} 0 & \dots & e^{-iA_{2\pi}} \\ e^{-iA_{2\pi/L_x}} & 0 & \dots \\ \dots & e^{-iA_{4\pi/L_x}} & \dots \\ \dots & \dots & \dots \\ \dots & \dots & e^{-iA_{(L_x-1)\pi/L_x}} & 0 \end{pmatrix}. \quad (10)$$

Here, the index of the rows and columns are $k_x = 0, \frac{2\pi}{L_x}, \dots, 2\pi - \frac{2\pi}{L_x}$. The eigenstates of the \bar{X} operator

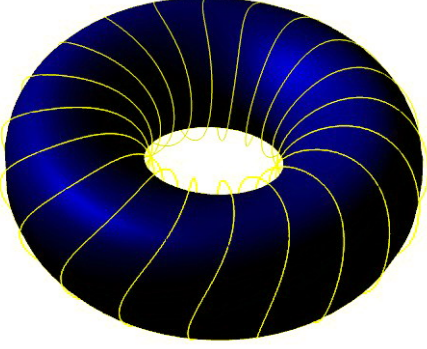


FIG. 1. (Color online) Shift of the Wannier polarization as k_y varies. The azimuthal direction represents the real space x while the poloidal direction represents the periodic domain of k_y . For any full rotation along y , i.e. $k_y \rightarrow k_y + 2\pi$, the Wannier state shifts by $x \rightarrow x + 1$.

form an orthogonal complete basis. Due to the simple form of \bar{X} in momentum space, one can prove that the eigenstates of \bar{X} are Wannier states defined in Eq. (4), with the phase $\varphi_{\mathbf{k}}$ defined by

$$|W_{nk_y}\rangle = \frac{1}{\sqrt{L_x}} \sum_{k_x} e^{-ik_x n} e^{i\varphi_{\mathbf{k}}} |\mathbf{k}\rangle, \quad (11)$$

$$\varphi_{\mathbf{k}} = - \sum_{0 \leq p_x < k_x} A_{p_x k_y} - k_x P_x(k_y),$$

with

$$P_x(k_y) = -\frac{1}{2\pi} \sum_{0 \leq p_x < 2\pi} A_{p_x k_y}.$$

This definition is periodic in $k_x \rightarrow k_x + 2\pi$. The corresponding eigenvalues are

$$\bar{X} |W_{nk_y}\rangle = e^{i\frac{2\pi}{L_x}(n+P_x)} |W_{nk_y}\rangle. \quad (12)$$

Therefore, we see that the center-of-mass (CM) position of the state $|W_{nk_y}\rangle$ is shifted by P_x away from the lattice site position n . This fact indicates that $P_x(k_y)$ has the physical meaning of charge polarization³⁶. In the large L_x limit, $A_{\mathbf{k}} \rightarrow \frac{2\pi}{L_x} a_x$ and $P_x(k_y) = -\frac{1}{2\pi} \int_0^{2\pi} a_x dk_x$. Since $P_x(k_y)$ is a $U(1)$ phase for each k_y , one can define its winding number when k_y goes from 0 to 2π :

$$C_1 = \sum_{n=1}^{L_y} \frac{i}{2\pi} \log \left(e^{i2\pi[P_x(2\pi n/L_y) - P_x(2\pi(n-1)/L_y)]} \right). \quad (13)$$

The log function is defined to take the value of the phase difference $2\pi [P_x(2\pi n/L_y) - P_x(2\pi(n-1)/L_y)]$ in the region of $[-\pi, \pi)$. As long as L_y is not too small so that $P_x(k_y)$ would not jump by an integer between two neighboring k_y values, the C_1 obtained agrees with the Chern number in the large L_y limit.

For $C_1 \neq 0$, the Wannier states $|W_n(k_y)\rangle$ have a ‘‘twisted boundary condition’’ in k_y , since $P_x(k_y + 2\pi) =$

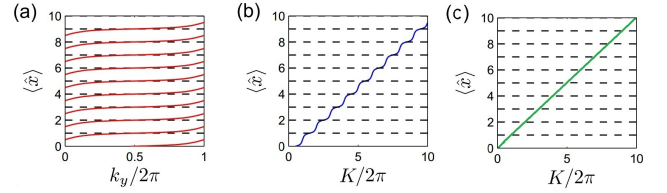


FIG. 2. (Color online) Wannier center evolution of the Dirac model used in Ref. 25 from $x = 0$ to $x = 10$ as a function of (a) $k_y/2\pi$ and (b) of the extended wave vector $K/2\pi$. From (a) to (b), it becomes visible how the evolution of x changes as a function of K , suggesting its similarity to Landau level wave functions (c).

$P_x(k_y) + C_1$, such that $|W_n(k_y + 2\pi)\rangle = |W_{n+C_1}(k_y)\rangle$. As is illustrated in Fig. 1, for $C_1 = 1$ the Wannier state CM position $x_n(k_y) = n + P_x(k_y)$ forms a helical curve on the parameter space torus of x, k_y . The key observation which enables the Wannier state representation of FCI is the fact that the twisted boundary condition allows to label all Wannier states in such a 2D system by a 1D parameter. If we define

$$|W_{k_y+2\pi n}\rangle = |W_{n,k_y}\rangle, \quad \text{for } k_y \in [0, 2\pi), \quad (14)$$

it yields $|W_K\rangle$, with $K = k_y + 2\pi n$ a continuous function of K (in the large L_y limit). The CM position $x_K = \langle W_K | \bar{X} | W_K \rangle = e^{i\frac{2\pi}{L_x}(n+P_x(k_y))}$ for $K \in [2\pi n, 2\pi(n+1))$ is continuous in K and satisfies $x_{K+2\pi} = x_K + 1$. In this sense, x_K increases linearly with K (Fig. 2).

Due to this behavior of $|W_K\rangle$, an exact mapping can be defined between the Wannier states in the $C_1 = 1$ FCI and the LLL states in a FQH problem. Consider a spinless fermion with the Hamiltonian $H = \frac{1}{2m}(\mathbf{p} - \mathbf{A})^2$ on a torus of the size $L_x l_B \times L_y l_B$ with the uniform perpendicular magnetic field $\nabla \times \mathbf{A} = B = 2\pi/l_B^2$. The total number of flux is $N_\Phi = L_x L_y$, so that the LLL contains the same dimension of Hilbert space as the lattice model discussed above on a lattice of the size $L_x \times L_y$. In a gauge choice $A_x = 0$, $A_y = Bx$, the LLL wave functions have the form

$$\begin{aligned} \psi_K(x, y) &= \frac{1}{\sqrt{2\pi l_B^2}} \sum_{n \in \mathbb{Z}} e^{iKy/l_B - \pi \left(\frac{x}{l_B} - \frac{K}{2\pi} - nL_x \right)^2} \\ &\equiv \frac{1}{\sqrt{2\pi l_B^2}} e^{iKy/l_B - \pi \left(\frac{x}{l_B} - \frac{K}{2\pi} \right)^2} \\ &\quad \cdot \vartheta \left(-iL_x \left(\frac{x}{l_B} - \frac{K}{2\pi} \right) \middle| iL_x^2 \right) \end{aligned} \quad (15)$$

with $\vartheta(z|\tau)$ the Jacobi theta function³⁷ which are appropriate superpositions of the cylindric wave functions.

Notice that we have defined the momentum K slightly differently from the usual definition used in Ref. 25 and 38 and in the subsequent sections, so that here K is dimensionless and given by $K = \frac{2\pi}{L_y} n$, $n \in \mathbb{Z}$ on the $L_x l_B \times L_y l_B$ torus. This definition leads to identical results as the usual definition used later if we replace the l_B here by $\sqrt{2\pi} l_B$.

For $L_x \gg 1$, this wave function is a Gaussian function around the CM position $x_K = K \frac{L_x}{2\pi}$. Denoting $|\psi_K\rangle$ as the state corresponding to wave function $\psi_K(x, y)$, one can define a unitary mapping between the Hilbert spaces of the Landau level and the lattice C_1 Chern insulator:

$$\begin{aligned} f : \text{H}_{\text{CI}} &\longrightarrow \text{H}_{\text{LLL}}, \\ f(|W_K\rangle) &= |\psi_K\rangle, \end{aligned} \quad (16)$$

with H_{CI} and H_{LLL} denoting the Hilbert spaces of the CI and LLL, respectively. Such a mapping preserves the continuity in K and also the topological properties of $|W_K\rangle$ and $|\psi_K\rangle$, i.e., their winding while momentum K is increased. Using the reverse map f^{-1} , the many-body states of the LLL, such as Laughlin states and other FQH states defined in the LLL, can all be mapped to corresponding states in the FCI. Similarly, a Hamiltonian H of a FQH system can also be mapped to a corresponding Hamiltonian $H_{\text{FCI}} = f^{-1}Hf$. The main purpose of the current paper is to study the Hamiltonians H_{FCI} which are mapped from the PP Hamiltonians in the FQH system. One can also perform the reverse, mapping the FCI Hamiltonian such as a Hubbard type interaction H_U of the lattice fermions to a FQH Hamiltonian $H_{\text{FQH}} = fH_U f^{-1}$. More details of such a mapping will be evaluated in the following sections.

There is a subtle point that we want to discuss before ending this section. The definition of maximally localized Wannier states in Eq. 11 still leave an ambiguity in the relative phase between different $|W_{nk_y}\rangle$. If we redefine $|W_{nk_y}\rangle \rightarrow e^{i\theta_{k_y}} |W_{nk_y}\rangle$ with any phase θ_{k_y} , all the properties discussed above remain the same. The map f , however, depends on this choice and different choices of phase corresponds to physically different mappings between FCI and FQH systems. To preserve the locality in the mapping, a choice should be made which makes $|W_{nk_y}\rangle$ continuous in k_y in the large L_y limit. An example of the choice is the following³⁹:

$$\begin{aligned} \theta_{k_y} &= - \sum_{0 \leq p_y < k_y} A'_{p_y} - k_y P_{y0}, \\ P_{y0} &= -\frac{1}{2\pi} \sum_{0 \leq p_y < 2\pi} A'_{p_y}, \\ A'_{p_y} &= -\text{Im} \log \left(\sum_{\alpha} u_{0, p_y + \frac{2\pi}{L_y}, \alpha}^* u_{0, p_y, \alpha} \right). \end{aligned} \quad (17)$$

In the $L_y \rightarrow \infty$ limit, $A'_{p_y} \simeq a_y(0, p_y) \frac{2\pi}{L_y}$. This choice of θ_{k_y} corresponds to a gauge transformation which makes $a_y(\mathbf{k})$ uniform along the $k_x = 0$ line. Any other gauge choice $\theta'_{k_y} = \theta_{k_y} + \delta\theta_{k_y}$ also works and describes topologically equivalent states, as long as $\delta\theta_{k_y}$ is a smooth periodic function of k_y in the large L_y limit. While different gauge choices $\delta\theta_{k_y}$ of the Wannier states do not change the topological universality class of the associated state, it can be used as variational parameters in the many-body ground state and can be optimized numerically by the comparison of the Wannier ground state with the exact ground state.^{26,27}

III. PSEUDOPOTENTIAL REPRESENTATION OF INTERACTIONS

In this section, we review the PP representation of interactions in FQH systems, and then map it to the FCI using the map established in (16). The PP approach was pioneered by Haldane in the context of FQHE²⁸: Suppose we assume all relevant degrees of freedom to be located in the LLL. When projected onto this subspace, which is a perfectly flat band, the kinetic energy is frozen out and the Hamiltonian thus consists only of an interaction term reminiscent of the Coulomb interaction

$$H = \sum_{i < j} V(\mathbf{r}_i - \mathbf{r}_j), \quad (18)$$

where the sum extends over all pairs of particles. This means that the interaction is fully characterized by its interaction energy between the particles i and j . The PPs are then defined by

$$H = \sum_{i < j} \sum_{m=0}^{\infty} V^m P_{ij}^m, \quad (19)$$

where P_{ij}^m projects onto a state where particles i and j have relative angular momentum m and V^m is the energy penalty for having two particles in such a state, taking on odd values $m = 1, 3, \dots, 2M + 1$ for fermions and even values $m = 0, 2, \dots, 2M$ for bosons. Since the LLL is perfectly flat, the m index also characterizes the distance between the particles. As the interactions are of repulsive Coulomb type, we can make the V^m s positive semidefinite by also fixing them to be real. This pseudopotential construction is particularly elegant on the infinite plane and the sphere where it was first defined^{28,40}, where translational symmetry and rotational symmetry are preserved and the relative angular momentum of a two-electron state is thus a well-defined quantum number. In particular, this construction allows for a most explicit connection between the Hamiltonian and the clustering properties of quantum Hall wave functions. For the Laughlin state wave function at $\nu = 1/3$ filling, where⁷ $|\Psi_L\rangle \sim \prod_{i < j} (z_i - z_j)^3$, the wave function decays as the 3rd power as two particles approach each other. This shows that two electrons are never allowed in a relative angular momentum state of $m = 1$, i.e. the particles maximally avoid each other within a featureless liquid state²⁸. It follows that $|\Psi_L\rangle$ is located in the nullspace of $H_{\text{Laughlin}} = \sum_{i < j} V_1 P_{ij}^1$. Furthermore, the Hilbert space at the appropriate filling only allows for one state of such a kind on a trivial genus manifold, implying that $|\Psi_L\rangle$ is the exact unique ground state of H_L . Similar trial Hamiltonian constructions are allowed for many other states, including non-Abelian quantum Hall states such as the Read-Rezayi series and others^{30,31,41}.

The Landau level on a cylinder can be seen as a hybrid version of the spherical and planar scenario. Starting from a Cartesian (x, y) plane, we impose periodic boundary conditions along y and, in analogy to the sphere,

quantize the pseudo-momentum along y according to the total magnetic flux N_ϕ , constraining the available area for the guiding center motion. We assume an infinite cylinder along the x -direction. On the cylinder geometry, the PP Hamiltonian takes the explicit form⁴²

$$H = \gamma \sum_{i < j} \sum_{n, m} \int dq l_B V^m L_m(q^2 l_B^2 + \gamma^2 n^2) e^{-q^2 l_B^2 / 2} \times e^{-\gamma^2 n^2 / 2} e^{i\gamma n \hat{x}_i / l_B} e^{iq(\hat{y}_i - \hat{y}_j)} e^{-i\gamma n \hat{x}_j / l_B}, \quad (20)$$

where γ is the aspect ratio of the cylinder, l_B is the magnetic length, q denotes the momentum variable along x , V^m is the PP energy of a state with relative angular momentum m , and L_m denotes the m th Laguerre polynomial³⁷. (Note that we have explicitly included all units in (20) as compared to Ref. 42.) Eq. 20 gives a pair interaction energy for each m . In the plane limit where $\gamma n \rightarrow k_x l$, the sum over n reduces to a momentum integral along y analogous to the q integration along x , resulting in a two-dimensional momentum integral which reduces to the pair interaction

$$V(\mathbf{r}_i - \mathbf{r}_j) = \sum_m V^m P^m(\mathbf{r}_i - \mathbf{r}_j) = \sum_m V^m L_m(-l_B^2 \nabla^2) \delta^2(\mathbf{r}_i - \mathbf{r}_j). \quad (21)$$

This decomposition is valid for sufficiently short-ranged

potentials $V(\mathbf{r}_i - \mathbf{r}_j)$. Note that the functional form of Eq. 21 is different from that in Ref. 42 because we have used ordinary coordinates instead of guiding center coordinates. If one replaces all coordinates including their derivatives with their guiding center analogues, $l_B^2 \delta^2(\mathbf{r}_i - \mathbf{r}_j)$ will be replaced by the exponential tail expression $e^{-|\mathbf{r}_i - \mathbf{r}_j|^2 / 2l_B^2}$ in Ref. 42. The details of this calculation are shown in Appendix A.

For later purposes, we also Fourier transform Eq. 21 and invoke the orthogonality relation of the Laguerre polynomials (see also Appendix B) to obtain

$$V^m = 4\pi l_B^2 \int \frac{d^2 k}{(2\pi)^2} e^{-l_B^2 k^2} L_m(k^2 l_B^2) V(k). \quad (22)$$

The above expression, which will also be rederived in Appendix B as a special case of a much more general result obtained from first principles, enables us to compute the PP coefficients V^m directly from a generic potential $V(k)$. It is the starting point for the generalization to interactions involving more than two bodies, as is described in Section VI.

To apply the PP decomposition to an FCI system with periodic boundary conditions in both directions, we have to compactify the open direction of the cylinder. The single particle states on the torus are the $\psi_K(x, y)$ defined in Eq. 15. In this basis, the m th PP Hamiltonian has the matrix elements

$$U_{n_1, n_2, n_3, n_4}^m = \int d^2 \mathbf{r}_i d^2 \mathbf{r}_j (\psi_{n_1}(\mathbf{r}_i)^* \psi_{n_2}(\mathbf{r}_j)^* - \psi_{n_2}(\mathbf{r}_i)^* \psi_{n_1}(\mathbf{r}_j)^*) U^m(\mathbf{r}_i - \mathbf{r}_j) (\psi_{n_3}(\mathbf{r}_i) \psi_{n_4}(\mathbf{r}_j) - \psi_{n_4}(\mathbf{r}_i) \psi_{n_3}(\mathbf{r}_j)). \quad (23)$$

U^m refers to a normalized PP that has nonzero projection only in the m th relative angular momentum sector. They form a basis in which a generic potential V is expanded. As such, the V^m s which appear in Eq. 22 and other places below refer to the component of V proportional to U^m , i.e. projected onto the relative angular momentum sector m . For simplicity, we have denoted $\psi_{K=2\pi n/L_y}(\mathbf{r})$ as $\psi_n(\mathbf{r})$, $n = 1, 2, \dots, L_x L_y$.

We can use the map (16) defined in Sec. II to define the corresponding PP Hamiltonian in FCI, which has the second-quantized form

$$U^m = \sum_{n_1, n_2, n_3, n_4} a_{n_1}^\dagger a_{n_2}^\dagger U_{n_1, n_2, n_3, n_4}^m a_{n_3} a_{n_4}, = \sum_{n+l_1 \in \mathbb{Z}, n+l_2 \in \mathbb{Z}} U_{l_1 l_2}^m a_{n+l_1}^\dagger a_{n-l_1}^\dagger a_{n-l_2} a_{n+l_2}. \quad (24)$$

Here,

$$a_n = \sum_{i, \alpha} \langle W_{2\pi n/L_y} | i\alpha \rangle c_{i\alpha} \quad (25)$$

is the annihilation operator of the Wannier state $|W_{2\pi n/L_y}\rangle$. The matrix element $U_{n_1 n_2 n_3 n_4}^m$ is simplified to the form of $U_{l_1 l_2}^m = U_{n+l_1, n-l_1, n-l_2, n+l_2}^m$ due to

the magnetic translation symmetry. (More discussion on the magnetic translation symmetry will be presented in Sec. V.) Depending on whether we consider the torus or cylinder geometry, the sites along the main cylinder axis labelled by n are assumed to obey periodic or open boundary condition, respectively. For the cylindrical case, Eq. 24 can be brought into a bosonic pair creation form given by $U_{l_1 l_2}^m = g\kappa^3 b_{l_1}^m b_{l_2}^m$, where

$$b_l^{2j+1} = l e^{-\kappa^2 l^2} \sum_{p=0}^j \frac{(-2)^{3p-j} (\kappa l)^{2p} \sqrt{(2j+1)!}}{(j-p)!(2p+1)!} \quad (26)$$

so that

$$U^m = g\kappa^3 \sum_n \hat{b}_n^{m\dagger} \hat{b}_n^m, \quad (27)$$

where $\hat{b}_n^m = \sum_{n+l \in \mathbb{Z}} b_l^m a_{n-l} a_{n+l}$. Here, $g = \frac{4V_0}{(2\pi)^{3/2}}$ is a constant with units of energy and $\kappa = \frac{2\pi l_B}{L_y} = \frac{1}{L_y}$. l_B has been set to $\frac{1}{2\pi}$ lattice constants in the latter equality in accordance to Ref. 25. In the following, l_B will be expressed in units of the lattice constant unless it appears

in the combination $l_B^2 \nabla^2$ or $l_B^2 q^2$, where q is a momentum variable. The complete derivation of Eq. 27 can be found in Appendix C.

The Hamiltonian in (24) will be the starting point of Sec. IV when we expand different FCI models into this PP form. Its $m = 1$ case has been previously used to define low-dimensional Mott-type models with bare onsite hardcore potentials at fractional filling^{38,43}. The PP U_{tor}^m on the torus can be found by summing over all the periodic images of $U_{l_1 l_2}^m$ (referred to as U_{cyl}^m in Appendix D) satisfying $l_1 + l_2 \bmod 2L_x L_y = 0$. This constraint can be generalized to the case with more than two bodies, as shown in Appendix E.

For finite-size investigations on the cylinder or the torus, we have to keep in mind that relative angular momentum is no longer a well-defined quantum number, as opposed to the case of the sphere or the plane. The parameter m in (21), which corresponds to the exact relative angular momentum as we take the planar limit, determines the order of the derivative acting on the hardcore potential via the degree of the Laguerre polynomial. This corresponds to a Taylor expansion of the interaction in momentum space⁴⁴. While its interpretation as the exact relative angular momentum is absent, it can still be employed as an expansion parameter for short-range interactions on a sufficiently large torus or cylinder. To see this in terms of the Hilbert space basis, we describe relative motion states on the torus by relative motion states on the plane. The latter can be exactly classified via the relative angular momentum m which is proportional to the interparticle distance in that relative state r_m . For $r_m/L_x, r_m/L_y \ll 1$, the overlap of the torus and planar relative motion states goes to unity, effectively reestablishing the notion of torus relative angular momentum for short distances. Still, this approximation becomes invalid for higher values of relative angular momentum. At the Hamiltonian level, this is reflected by the overcompleteness of the PPs U^m . This occurs because the interparticle distance $r_m \sim L_x, L_y$ that characterizes a relative angular momentum state will no longer be well-defined when r_m is comparable to the system lengths of the torus. A quantitative treatment of the overcompleteness bounds can be found in Appendix D.

A deep insight to note is that even though an exact angular momentum quantum number cannot be defined, the clustering property of the quantum Hall-type wave functions are still fixed appropriately at these finite size manifolds such that they can be *exactly* located in nullspaces of PP Hamiltonians. This was elegantly shown for the torus by Haldane and Rezayi²⁹, which we illustrate for the U_1 PP at $\nu = 1/3$ filling: demanding that the many-particle ground state pays no energy due to U_1 , it necessitates that the wave function decays to third power as the particles approach each other. Oddness due to fermionic statistics and boundary conditions on the torus automatically restricts the functional form of the wavefunction to be $\Psi \sim \prod_{i < j} \vartheta(z_i - z_j | \tau)^3$, where ϑ is the odd Jacobi theta function. The groundstate is thus

forced to be of Laughlin type. This fixes $N_\phi - 3$ zeroes of the wave function, where the remainder 3 constitute the topological center of mass degeneracy of the Laughlin state⁴⁵. A similar discussion can be pursued for the cylinder, where the center of mass degeneracy is absent but the clustering property of the wave function leads to the same finding for the remainder functional form of the wave function⁴⁶.

All in all, the properties of the pseudopotential expansion sets the stage for numerical investigations of short-ranged interactions of FCIs as well as the defining of trial Hamiltonians for new quantum Hall-type fractional Chern phases, both of which will be pursued in the following.

IV. PSEUDOPOTENTIAL EXPANSION OF FRACTIONAL CHERN INSULATORS

A. Model Hamiltonians

We apply the PP expansion to two model FCI Hamiltonians, the checkerboard (CB) model introduced in Ref. 17 and the honeycomb (HC) model introduced in Refs. 6 and 47. Both models possess an almost flat (dispersionless) band which mimics the LLL in an FQH system. There, the Coulomb-type electron interactions lift the macroscopic degeneracy of the LLL, leading to a topologically degenerate groundstate. In the same spirit, we add Hubbard-type interaction terms to our model Hamiltonians such that

$$\begin{aligned} H_{\text{int}} &= \lambda H_{NN} + (1 - \lambda) H_{NNN} \\ &= h_0 \left(\lambda \sum_{\langle ij \rangle} n_i n_j + (1 - \lambda) \sum_{\langle\langle ij \rangle\rangle} n_i n_j \right), \\ H &= H_0 + H_{\text{int}}, \end{aligned} \quad (28)$$

where λ characterizes the relative strengths of the nearest neighbor (NN) and next-nearest-neighbor (NNN) interaction terms. h_0 , a parameter with units of energy, sets the overall magnitude of H_{int} . The single-particle term H_0 gives rise to the almost flat band and provides information for the construction of the Wannier basis. This is the basis we will use for expressing the two-body interacting term H_{int} in the same basis as the PP Hamiltonians U^1, U^3 , etc. as denoted in (24).

We consider interactions that are much larger than the bandwidth of the almost flat band, but much smaller than the interband gap. In this limit, for a partially filled flat band, we can ignore the coupling to the upper band and only study the effect of interactions in the subspace of the flat band. With this picture in mind, we expand H_{int} in terms of the PPs in the Wannier basis of the partially filled band. As long as the bandwidth of the almost flat band is much smaller than the interaction strength, we can ignore the bandwidth and consider only the interaction term.

The checkerboard (CB) lattice model consists of two interlocking square lattices displaced $(1/2, -1/2)$ sites relative to each other (Fig. 3). Its noninteracting Hamiltonian H_0^{CB} consists of NN, NNN and NNNN hopping terms parametrized by hopping strengths t , t' , and t'' respectively⁴⁸. The NN hoppings exist between sites belonging to different sublattices and carry a phase ϕ , giving rise to the time-reversal symmetry breaking necessary for a nonzero Chern number. Both the NN and NNNN hoppings exist between different sublattices, leading to off-diagonal terms in the single-particle (noninteracting) Hamiltonian. In sublattice space,

$$H_0^{\text{CB}}(k) = d_0 I + \sum_i d_i \sigma_i, \quad (29)$$

where

$$d_1 = -4t \cos \phi \cos \frac{k_x}{2} \cos \frac{k_y}{2},$$

$$d_2 = -4t \sin \phi \sin \frac{k_x}{2} \sin \frac{k_y}{2},$$

$$d_3 = -2t'(\cos k_x - \cos k_y).$$

The expression for d_0 is irrelevant because it is not needed for the computation of the Wannier basis. We set $t = 1$, $t' = -t'' = 1/(2 + \sqrt{2})$ and $\phi = \pi/4$ as in Ref. 17 to achieve the maximal the flatness ratio of ~ 30 for the bottom band. We can explicitly see why a nonzero ϕ is necessary for having a topologically nontrivial model: as the Chern number is given by $C_1 = \frac{1}{4\pi} \int d^2 \vec{k} \vec{d} \cdot (\partial_x \vec{d} \times \partial_y \vec{d})$, it can only be nonzero if none of the d_i 's is identically zero.

Notice that H_0^{CB} is not of Bloch form since the d_i 's do not obey the periodicity of 2π . This is because some sites are noninteger lattice spacings away from each other (Fig. 3). We can remedy this by shifting one sublattice site on top of the other within a unit cell. Mathematically, this corresponds to a gauge transformation of $c_{kB}^\dagger \rightarrow c_{kB}^\dagger e^{-i(k_x - k_y)/2}$ where B refers to one of the sites within the sublattice. After the gauge transformation,

$$d_1 = -t[\cos \phi + \cos(k_x + k_y + \phi) + \cos(k_x - \phi) + \cos(k_y - \phi)],$$

$$d_2 = -t[\sin \phi + \sin(k_x + k_y + \phi) + \sin(k_x - \phi) + \sin(k_y - \phi)],$$

$$d_3 = -2t'(\cos k_x - \cos k_y).$$

The noninteracting part of the honeycomb model is defined similarly. The unit cell consists of two adjacent sites. The phase ϕ is carried between NNN sites, which lie in the same sublattice. NNNN interactions which occur for diametral sites on the same hexagon involve different sublattices (Fig. 3). After an analogous gauge transformation,

$$H_0^{\text{HC}}(k) = d_0 I + \sum_i d_i \sigma_i, \quad (30)$$

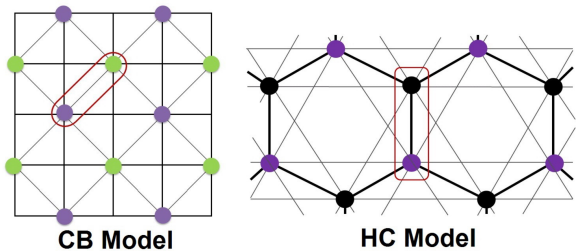


FIG. 3. (Color online) Lattice structure of the CB(left) and HC (right) models. Sites colored differently belong to different sublattices. The unit cells are demarcated in red. For the CB model, NN interactions are between different sublattices while NNN and NNNN interactions occur within the same sublattice. For the HC model, both the NN and NNNN interactions occur between different sublattices, but the NNN interactions act within the same sublattice.

where

$$d_1 = -t(1 + \cos k_x + \cos k_y) - t''(\cos(k_x + k_y) + 2 \cos(k_x - k_y)),$$

$$d_2 = t(\sin k_x + \sin k_y) + t'' \sin(k_x + k_y),$$

$$d_3 = 2t' \sin \phi (\sin k_y - \sin k_x + \sin(k_x - k_y)).$$

The values for the NN, NNN, and NNNN hoppings are given by $t = 1$, $t' = 0.6$, and $t'' = -0.58$, $\phi = 0.4\pi$ such that the flatness ratio of the band is optimized to about 60⁴⁷. We stress that while the optimization of these flatband parameters is not necessary for performing the PP expansion, it is physically relevant in increasing the stability of an FQH state present in the system.

B. Expressing H_{int} in the Wannier basis

We now have the necessary ingredients for expressing the interaction part of our model Hamiltonians in the same basis as the PPs in FQHE. First, we can perform a Fourier transform on H_{int} such that it becomes

$$\begin{aligned} H_{\text{int}} &= \lambda h_0 \sum_{\langle ij \rangle} n_i n_j + (1 - \lambda) h_0 \sum_{\langle\langle ij \rangle\rangle} n_i n_j \\ &= \sum_q V^{\alpha\beta}(q) n_{-q\alpha} n_{q\beta}, \end{aligned} \quad (31)$$

where q is an internal momentum variable, α, β are the sublattice indices, and $n_{q\alpha} = \sum_{k_x k_y} c_{k+q, \alpha}^\dagger c_{k\alpha}$. $V^{\alpha\beta}(q)$ denotes the q th Fourier component of the interaction between the sublattice index α and β . This is an expression quartic in the creation and annihilation operators c, c^\dagger in the momentum/sublattice basis. Since we are only considering interactions within the flat band, we project out the upper band and keep only the matrix elements of $n_{q\alpha}$ in the flat band. After projecting out the upper band,

the annihilation operator $c_{k\alpha}$ can be expanded in the Wannier state basis:

$$\begin{aligned} c_{\vec{k}\alpha} &= \sum_n \langle \vec{k}\alpha | W_{2\pi n/L_y} \rangle a_n + \text{upper band contributions} \\ &\rightarrow \sum_n \langle \vec{k}\alpha | W_{2\pi n/L_y} \rangle a_n \\ &=: \sum_n U_{xk_x\alpha k_y} a_{x,k_y}, \end{aligned} \quad (32)$$

since $\frac{2\pi n}{L_y} = K = k_y + 2\pi x C_1 = k_y + 2\pi x$. In this representation, the density operator becomes

$$\begin{aligned} n_{q\alpha} &= \sum_{k_x k_y} L_x^{-1/2} c_{k+q,\alpha}^\dagger c_{k\alpha} \\ &= \sum_{k_x k_y} L_x^{-1/2} \sum_{x_1} U_{x_1, k_x+q_x, \alpha, k_y+q_y}^* a_{x_1, k_y+q_y}^\dagger \\ &\quad \sum_{x_2} U_{x_2 k_x \alpha k_y} a_{x_2 k_y} \\ &= \sum_{k_y x_1 x_2} N_{q\alpha x_1 x_2 k_y} a_{x_1, k_y+q_y}^\dagger a_{x_2 k_y}, \end{aligned} \quad (33)$$

where the normalization factors $N_{q\alpha x_1 x_2 k_y}$ follow from (32). We obtain

$$\begin{aligned} H_{\text{int}} &= \sum_{q\alpha\beta} V_q^{\alpha\beta} n_{-q,\alpha} n_{q\beta} \\ &= \sum_{q_x} \sum_{\{x_j\}, \{K_j\}, \alpha\beta} V_q^{\alpha\beta} \delta_{q_y - k_{2y} + k_{1y}} \delta_{k_{2y} - k_{1y} - k_{3y} + k_{4y}} N_{-q\alpha x_1 x_2 k_{2y}} N_{q\beta x_3 x_4 k_{4y}} a_{K_1}^\dagger a_{K_2} a_{K_3}^\dagger a_{K_4} \\ &= \sum_{K_1 K_2 K_3 K_4} (h^{\text{int}})_{K_1 K_2 K_3 K_4} a_{K_1}^\dagger a_{K_2} a_{K_3}^\dagger a_{K_4} \\ &\simeq - \sum_{n'n} \sum_{l_1 l_2} f(n, n', l_1, l_2) (a_{(n-l_1)/2} a_{(n+l_1)/2})^\dagger (a_{(n'-l_2)/2} a_{(n'+l_2)/2}). \end{aligned} \quad (34)$$

A quadratic term has been dropped in the final step because it can be absorbed into the noninteracting part of the Hamiltonian. The latter is irrelevant for our current purpose of expressing the interaction operator in the Wannier basis. Note, however, that this quadratic term should not be omitted if we were to perform studies on energetics. Due to fermionic statistics of the $c_{n\pm l}$ operators, we can antisymmetrize H_{int} , leading to the matrix elements

$$\begin{aligned} h(n, n', l_1, l_2) &= f(n, n', l_1, l_2) - f(n, n', -l_1, l_2) \\ &\quad - f(n, n', l_1, -l_2) + f(n, n', -l_1, -l_2), \end{aligned} \quad (35)$$

which are manifestly antisymmetric in l_1 and l_2 , just like the PPs $U_{l_1 l_2}^m$. We see from Eq. 34 that $h(n, n', l_1, l_2)$ corresponds to a pair hopping interaction on a line. Two particles with the CM ‘‘position’’ n' separated by l_2 sites simultaneously hop onto new positions with CM position n separated by l_1 sites (see also Fig. 7). More discussions

on the physical interpretation of this interaction will be presented in Section V.

C. Pseudopotential expansion of the interaction term

While the PP matrix elements $U_{l_1 l_2}^m$ depend only on l_1 and l_2 , the FCI interaction Hamiltonian matrix elements in the Wannier basis $h(n_1, n_2, l_1, l_2)$ also depend on n_1 and n_2 . As a consequence, only a part of $h(n_1, n_2, l_1, l_2)$ can be expanded in terms of PPs. This important fact can be understood in terms of magnetic translation (MT) symmetry breaking, which will be analysed in depth in the next section. Here, we shall concern ourselves with the terms that can be expanded in PPs, defined by

$$H_p(n, n', l_1, l_2) = \frac{\delta_{nn'}}{2L_x L_y} \sum_{N=1}^{2L_y} h(N, N, l_1, l_2). \quad (36)$$

H_p vanishes for $n \neq n'$ and does not depend on n when $n_1 = n_2 = n$, as required. The sum runs from 1 to $2L_y$ because $h(n, n, l_1, l_2)$ is periodic in n with period $2L_x L_y$, as evident from the periodicity of $a_{(n \pm l)/2}$ in Eq. 34.

We would like to expand H_p in an orthonormal basis of PPs U^1, U^3 , etc. However, this expansion is only unique and thus meaningful if we include PPs with m bounded by a certain m_{\max} . This is because the inclusion of higher PPs can yield an overcomplete operator basis, a consequence of the finite size of the torus geometry explained in Section III. The truncated PP basis is no longer complete, but we can still perform a PP expansion of H_p (now suitable normalized) by writing

$$H_p = \sum_m^{m_{\max}} V^m U^m + H_{>} =: H_{\text{pseudo}} + H_{>}, \quad (37)$$

and finding the PP expansion coefficients V^m that maximize the normalized overlap $\langle H_p, H_{\text{pseudo}} \rangle$. The overlap is taken by summing over all $|l_1|, |l_2| \leq L_x L_y$ since H_p has a period of $2L_x L_y$. Specifically, for any two Hamiltonians H and H' that respect MT symmetry,

$$\langle H, H' \rangle = \frac{\sum_{l_1 l_2} H_{l_1 l_2} H'_{l_1 l_2}}{\sqrt{\sum_{l_1 l_2} H_{l_1 l_2}^2 \sum_{l_1 l_2} H'_{l_1 l_2}^2}}. \quad (38)$$

The term $H_{>}$ consists of the part of H_{int} that does not break MT symmetry, but still cannot be uniquely expressed in terms of the PPs. It includes, for instance, hoppings that occur over lengths comparable to the size of the torus.

When the U^m 's form an orthonormal basis, the V^m 's that maximize the normalized overlap $\langle H_p, H_{\text{pseudo}} \rangle$ can be determined as

$$V^m = \langle H_p, U^m \rangle.$$

From Fig. 4, we see that the percentage of H_p that can be expanded as PPs $\sum_{j=0}^{j_{\max}} |V^j|^2$ has the maximum value for 0.94 for the CB NNN interaction (Fig. 4). As expected, the first PP has the highest weight, which favors the possibility of simple FQH states such as Laughlin states. With the relative angular momentum m being proportional to interparticle distance, U^m is expected to decay faster with $|l_1|, |l_2|$ as m increases. This will be shown in more detail in Appendix C. It is notable, however, that the second neighbor coupling leads to a better overlap with the first PP than the nearest neighbor Hamiltonian. This indicates that the PP Hamiltonians mapped to FCI systems are not simple density-density interactions and their matrix elements in real space lattice site basis can exhibit a nonmonotonic dependence on distance. More specifically, this is because $U_{l_1 l_2}^1 \sim l_1 l_2$ is not strongly peaked around $l_1 = \pm l_2$ in $l_1 - l_2$ space, as shown in Fig. 5, unlike the NN interaction. Since $l_1 = \pm l_2$ corresponds to $q = 0$ (as defined in Eq. 34), we see that the NN terms are "too local" for a good overlap with U^1 .

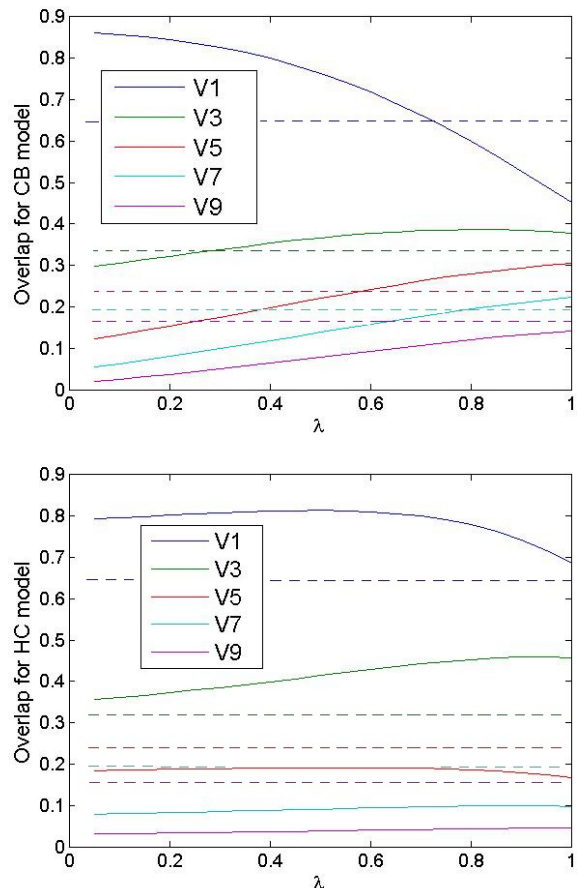


FIG. 4. (Color online) The pseudopotential expansion of the fermionic checkerboard (upper) and the honeycomb (lower) models for $L_x = L_y = 6$. The normalized overlap V^j is plotted against λ , where $H_{\text{int}} = \lambda H_{NN} + (1 - \lambda) H_{NNN}$, so that we have the NNN limit on the left and the NN limit on the right. For the CB model, we see that the NN and NNN terms exhibit marked differences in their pseudopotential expansions, with the MT symmetry conserving part of its NNN term consisting almost exclusively of the V^1 and V^3 terms. This can be understood by studying its distribution of matrix elements (Fig. 5). For comparison, the PP coefficients V^1 to V^9 of the QH Coulomb interaction are plotted as dashed lines. The NNN interaction has a larger V^1 coefficient and smaller V^3, V^5, \dots coefficients than the Coulomb interaction, and is hence even more likely to exhibit Laughlin groundstate.

In general, the matrix elements $U_{l_1 l_2}^m \sim (l_1 l_2)^m$, so U^m becomes more localized at $l_1 = \pm l_2$ for higher m .

For comparison, the pseudopotential coefficients for the Coulomb interaction in a QH system are also plotted in Fig. 4. They can be derived via Eq. 22, where $V(k) = \frac{4\pi}{k}$. We see that the PP coefficients of the FCI interactions do not differ too much from those of the Coulomb interaction, and in fact have a larger V^1 coefficient in a large range of λ .

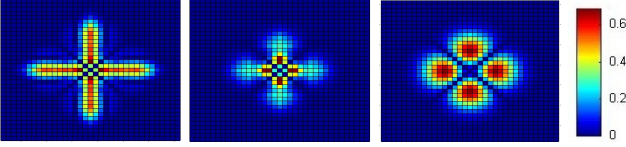


FIG. 5. (Color online) Plots of normalized $|H_p|$ for the NN (left) and NNN (center) terms of for the fermionic CB model. The horizontal and vertical axes represent $l_1 - l_2$ and $l_1 + l_2$ respectively. Regions with relatively large $|H_p|$ are colored red. U^1 (right) is plotted for comparison. The NNN term evidently bears more resemblance to U^1 .

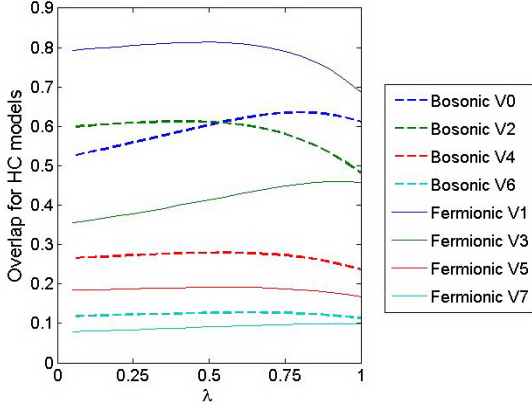


FIG. 6. (Color online) The pseudopotential expansion of the fermionic (solid line) and bosonic (dashed line) HC models for $L_x = L_y = 6$. The PP coefficient V^j is plotted against λ , where $H_{\text{int}} = \lambda H_{\text{NN}} + (1 - \lambda) H_{\text{NNN}}$, so that we have the NNN limit on the left and the NN limit on the right. The bosonic PP coefficients are in general closer to each other, with V^0 not larger than V^2 for some values of λ .

D. Fermion-Boson Asymmetry

In the quantum Hall effect, a Vandermonde determinant allows to equivalently switch from bosons to fermions which corresponds to an additional attachment of one flux per particle. This symmetry is broken in the fractional Chern insulator. We can see this explicitly by comparing the PP coefficients of both the fermionic and bosonic HC model. The latter model is also studied in other works like Ref. 47. The bosonic PPs are constructed analogously to the fermionic ones, except that they are now symmetrized instead of antisymmetrized (refer to Appendix C for more details).

The comparison between the PPs of the bosonic and fermionic HC models are displayed in Fig. 5. The bosonic PP coefficients are in general closer to each other, with V^0 not larger than V^2 . This is because of the large MT symmetry breaking (further described in the next section) that renders even the NN term rather nonlocal in the l_1, l_2 basis.

V. THE EFFECT OF MAGNETIC TRANSLATION SYMMETRY BREAKING

In this section, we analyze the origin of the terms in the FCI Hamiltonian that cannot be expanded into PPs. We review how magnetic translation (MT) symmetry in FQH system constrains the form of its two-body interaction terms, and investigate how this picture is generalized to the FCI case.

A. Origin of Magnetic Translation Symmetry breaking

Consider an $L_x l_B \times L_y l_B$ torus geometry which has been discussed in Sec. II. In the Landau gauge $A_x = 0$, $A_y = Bx$, the covariant momentum operators are $P_x = -i\partial_x$, $P_y = -i\partial_y - A_y$ which satisfies $[P_x, P_y] = iB$. The Hamiltonian $H = \frac{1}{2m} (P_x^2 + P_y^2)$ has two translation symmetries T_x^B, T_y^B defined by

$$\begin{aligned} T_x^B &= e^{i\frac{2\pi y}{L_y l_B}} e^{iP_x \frac{l_B}{L_y}}, \\ T_y^B &= e^{iP_y \frac{l_B}{L_x}}. \end{aligned} \quad (39)$$

T_y^B is an ordinary translation while T_x^B is a translation in x direction by l_B/L_y accompanied by a gauge transformation. The translation can only be defined in units of l_B/L_y so that the change of gauge potential $A_y = Bx \rightarrow B(x + l_B/L_y)$ can be cancelled by a gauge transformation. The action of T_x^B, T_y^B on the basis wavefunctions (15) is

$$\begin{aligned} T_y^B |\psi_K\rangle &= e^{iK/L_x} |\psi_K\rangle, \\ T_x^B |\psi_K\rangle &= \left| \psi_{K + \frac{2\pi}{L_y}} \right\rangle. \end{aligned} \quad (40)$$

For a general two-body interaction with H_{int} in the form of $H_{\text{int}} = \sum_{n_1, n_2, n_3, n_4} a_{n_1}^\dagger a_{n_2}^\dagger U^{n_1 n_2 n_3 n_4} a_{n_3} a_{n_4}$, the condition $[T_y^B, H_{\text{int}}] = 0$ requires $n_1 + n_2 = n_3 + n_4$, since $(T_y^B)^{-1} a_{n_1}^\dagger a_{n_2}^\dagger a_{n_3} a_{n_4} T_y^B = a_{n_1}^\dagger a_{n_2}^\dagger a_{n_3} a_{n_4} e^{2\pi i(n_1 + n_2 - n_3 - n_4)/L_x L_y}$. The condition $[T_x^B, H_{\text{int}}] = 0$ requires $U^{n_1 n_2 n_3 n_4} = U^{n_1+1, n_2+1, n_3+1, n_4+1}$. Therefore, the magnetic translation symmetry T_x^B and T_y^B determines the CM conservation ($n_1 + n_2 = n_3 + n_4$ or $n = n'$) and (one-dimensional) translation symmetry of the interaction Hamiltonian in FQH states, i.e., n -independence of the interaction matrix elements.

By comparison, in the lattice model, we only have the lattice translation symmetries which commute with each other. The action of the lattice translation T_x, T_y acts on the Wannier basis as

$$\begin{aligned} T_y |W_K\rangle &= e^{iK} |W_K\rangle, \\ T_x |W_K\rangle &= |W_{K+2\pi}\rangle. \end{aligned} \quad (41)$$

Comparing Eq. 41 with Eq. 40, we see that in the mapping from FCI to FQH defined in Sec. II, T_x, T_y is mapped

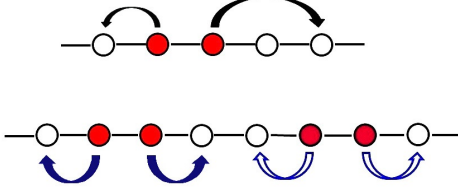


FIG. 7. (Color online) The two types of MT breaking hoppings. Top: A hopping process that changes the CM position. Bottom: Two hopping processes that preserve the CM position but break magnetic translation symmetry because the hopping at different CM position n (solid and hollow arrows) have different amplitude.

to $(T_x^B)^{L_y}$ and $(T_y^B)^{L_x}$, respectively. Therefore, in the lattice model, the translation symmetries only require the matrix element of two-body interaction $U^{n_1 n_2 n_3 n_4}$ to satisfy

$$\begin{aligned} U^{n_1 n_2 n_3 n_4} &= U^{n_1+L_y, n_2+L_y, n_3+L_y, n_4+L_y}, \\ U^{n_1 n_2 n_3 n_4} &= 0 \text{ if } n_1 + n_2 \neq n_3 + n_4 \pmod{L_y}. \end{aligned} \quad (42)$$

The magnetic translation symmetry breaking in the lattice models (Fig. 7) is also related to the non-uniform Berry curvature in momentum space. As was discussed in Sec. II, the CM position of the Wannier state $|W_K\rangle$ is determined by the flux of the Berry's phase gauge field $P_x(k_y)$. If the system has magnetic translation symmetry, $|W_K\rangle$ and $|W_{K+2\pi/L_y}\rangle$ are related by T_x^B , so that $P_x(k_y)$ must depend on k_y linearly. As a result, we expect MT symmetry breaking whenever the Berry curvature is nonuniform in momentum space, which is the case in a generic CI.

In addition, MT symmetry breaking will still be present even in the hypothetical case of perfectly flat Berry curvature. This is because the Wannier basis is not perfectly local. Recall from (34) that

$$n_1 + n_2 = n = k_{1y} + k_{2y} + (x_1 + x_2)L_y, \quad (43)$$

$$n_3 + n_4 = n' = k_{1y} + k_{2y} + (x_3 + x_4)L_y, \quad (44)$$

where the x_i s are the lattice sites of the original H_{int} . CM nonconserving terms occur where $x_1 + x_2 \neq x_3 + x_4$, when n and n' differ by a multiple of L_y . These terms do not appear in the original real-space basis where $H_{\text{int}} \propto \sum_{ij} n_i n_j = -\sum_{ij} c_i^\dagger c_j^\dagger c_i c_j$ annihilates and creates two particles at the same position. However, our Wannier basis functions generically have exponentially decaying tails on both sides of their peak \bar{x} , which produce CM nonconserving and thus MT breaking contributions.

B. Numerical results on MT symmetry breaking

We present the numerical results on MT symmetry breaking in our model Hamiltonians. Define the residual

$$H_{\text{res}}(n, n', l_1, l_2) = h(n, n', l_1, l_2) - H_p(l_1, l_2)$$

where, as before, $h(n, n', l_1, l_2)$ denotes the FCI interaction Hamiltonian expressed in the Wannier basis. H_{res} is the part of $h(n, n', l_1, l_2)$ which does not satisfy MT symmetry required by the PPs. Obviously, $H_{\text{res}} = 0$ if h is one of the PPs, since h will then be equal to H_p . The quantity

$$\delta_n^2 = \frac{\sum_{l_1 l_2, m} |H_{\text{res}}(m, m + nL_y, l_1, l_2)|^2}{\sum_{l_1 l_2, m, m'} |h(m, m', l_1, l_2)|^2}$$

allows us to track the origin of MT nonconservation. δ_0^2 comprises the elements of H_{res} satisfying $n = n'$. As defined in Eq. 36, these are the elements which are independent of n . δ_0^2 hence represents the fraction of matrix elements that are CM conserving but MT symmetry breaking. For $n \neq 0$, δ_n^2 represents MT nonconserving contributions that likewise do not respect CM conservation. δ_n^2 is plotted in Fig. 8 for various model Hamiltonians, for a system size $L_x = L_y = 6$. The results remain almost unchanged when L_x and L_y are varied as long as $L_x = L_y > 3$.

From the enhanced peak at $n = 0$, we conclude that most of the MT symmetry breaking occurs when CM is conserved. This happens because our maximally localized Wannier functions (WFs) are still mostly peaked at one site. The subdominant contributions from δ_n^2 for $n = \pm 1$ can be attributed to the finite tails of the WFs one site away from their center of mass. Indeed, δ_n^2 becomes exponentially small for $|n| > 1$. While the overall extent of MT symmetry breaking originates from the nonuniformity of the Berry curvature, its relative contribution to δ_n^2 for different n is dictated by the localization properties of the WFs.

C. Discussion on MT symmetry breaking

The decomposition of the FCI Hamiltonian into pseudopotentials is only exact in the thermodynamic LLL limit of zero bandwidth and homogeneous Berry curvature. For the generic model, the FCI Hamiltonian can only be partly decomposed into pseudopotentials, which we then discuss along general FQHE pseudopotentials on the cylinder or torus. From our calculations, the deviations are significant, suggesting that at least for the spectrum above the elementary low energy quasiparticle regime, there is no clear similarity between FCI and FQH systems. However, entanglement signatures of incompressible liquid phases, such as the entanglement spectrum⁴⁹ with the emergence of an entanglement gap⁵⁰,

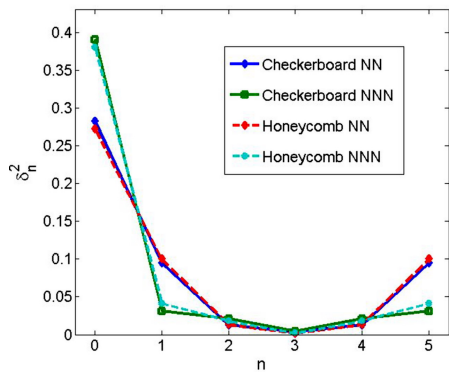


FIG. 8. (Color online) A plot of δ_n^2 for $L_x = L_y = 6$ for different model Hamiltonians. As evident from the dominance of the peak at $n = 0$, the amount of MT symmetry breaking largely stems from CM conserving terms. There is little difference between the degree of MT symmetry breaking in the different models.

show strong similarities of FCI ground states to their FQH analogues, even in terms of the counting rule of low-lying states^{21,33}. This is astonishing from the viewpoint of PPs, as the FCI and FQH models at the bare level could only possibly agree to the extent of the PP decomposable components of the FCI Hamiltonians.

Such an apparent discrepancy between analyses at the Hamiltonian and entanglement measure levels can be interpreted as a consequence of a renormalization group flow. As high energy modes are integrated out, the low energy physics of FCIs supposedly flows towards FQHE type scenarios, with reemergent symmetries such as magnetic translation group which is conserved in the FQHE but broken in the FCI at a bare level. Recast into pseudopotentials, it suggests that the PP non-decomposable part of the FCI Hamiltonian at the bare level should decrease upon renormalization, while the ratios of pseudopotentials of the PP-decomposable part of the bare interactions might deviate from the PP ratios in the low energy theory. This implies that even if two FCI Hamiltonians have similar PP ratios at the bare level, they can still differ considerably in their low energy description, and hence their propensity to host FQHE-type incompressible states (Fig. 8). This interpretation is consistent with the common theme from FQHE numerical studies that the data quality of entanglement spectra and its characterization of the bulk and edge mode properties is not significantly correlated to the spectral sharpness of the Hamiltonian spectrum, and partly anticipates the energy spectral flow⁵⁰. Ultimately, only the joint confirmation of both entanglement and Hamiltonian measures will justify true evidence for a fractional topologically ordered phase in the FCI models. From a low energy perspective, the seemingly clean finding from entanglement measures might not yet rule out that the inhomogeneous berry curvature induces a flow to a liquid different from FQHE, as may also be seen by hints such that the hierarchy liquid

construction cannot be established for the FCIs as in the FQHE case⁵¹. From the perspective of energetics, the effective pseudopotential weights of the FCI models in a low-energy theory are likely to be strongly modified due to "integrating out" the PP non-decomposable part of the bare model, which can also provide an explanation for the parameter trends of the stability of FCI phases as a function of system parameters⁵².

VI. MANY-BODY PSEUDOPOTENTIALS

A. Construction of many-body PP trial Hamiltonians

While we have only explored two-body interactions so far, PP expansions are also well-suited for many-body interactions. From the established knowledge in FQHE systems, it follows that various interesting FQAH liquids are located in the nullspace of certain many-body PPs. In theory, we can construct many-body FCI Hamiltonians that exhibit Pfaffian, Read-Rezayi etc. groundstates from such PPs^{30,31,41,53}.

The first task is to generalize Haldane's PPs for FCI models to more than two-body interactions⁵⁴. For two particles in the LLL and a translationally invariant potential $V(k) = \int e^{-ik \cdot r} V(r) dr$, the component projected on the m th Legendre component is given by Eq. 22

$$V^m = 4\pi l_B^2 \int \frac{d^2 k}{(2\pi)^2} e^{-l_B^2 k^2} L_m(l_B^2 k^2) V(k)$$

so that the m th pseudopotential (with $V^m \propto \delta_{mn}$) is given by $U^m(k) = V_0 L_m(l_B^2 k^2)$. As before, V_0 is a constant with units of energy. In the plane limit, the U^m s form an orthogonal basis which one can use to expand a generic potential profile.

When an interaction involves more than two particles, additional complications arise. To begin with, there are different ways of choosing to assign relative distance variables, or, angular momentum. (For two-body interactions, there is a unique assignment, as one degree of freedom drops out due the CM conservation.) When there are 3 particles, only one degree of freedom is eliminated due to CM conservation. As such, an ambiguity remains in choosing the many-body analog of relative angular momentum. This ambiguity is mathematically manifest when one tries to generalize Eq. 22. In the case of 3-body interactions, there will be integrals over both momenta k_1 and k_2 in the above expression, and one has to choose the new expression to involve $L_m(k_1^2)$, $L_m(k_2^2)$, $L_m((k_1 - k_2)^2)$, or a combination of these.

This formal ambiguity similar to coupling multiple angular momenta does not induce physical complications as we formulate generalized Haldane pseudopotentials (GHPs). Its detailed first-principle derivation can be found in Appendix B. We constrain ourselves to the application of GHPs to the total relative angular momen-

tum N -body PP Hamiltonians:

$$U^m(k) = L_m \left(\frac{k^2 l_B^2 N}{2(N-1)} \right). \quad (45)$$

Here, $U^m(k)$ is the N -body interaction potential that has a total relative angular momentum of m , with k being the momentum conjugate to the total relative coordinate w defined by

$$w = \frac{1}{N-1} \sum_{n=1}^{N-1} (z_n - z_N) = \frac{\sum_{i=1}^{N-1} z_i}{N-1} - z_N, \quad (46)$$

where $z_i = x_i - iy_i$ are the complex coordinates of the N particles.

In real space, the pseudopotential $U^m(w) \propto \int dk e^{ik \cdot w} U^m(k)$ depends explicitly on the positions of each of the N particles. If we select one of the N particles, the total relative angular momentum is the sum of the relative angular momenta of the other $N-1$ particles

$$\begin{aligned} & U_{n_1 n_2 n_3 n_4 n_5 n_6}^m \\ & \propto \sum_{\sigma} \int d^2 r_1 d^2 r_2 d^2 r_3 \psi_{n_1}^{\dagger}(r_1) \psi_{n_2}^{\dagger}(r_2) \psi_{n_3}^{\dagger}(r_3) L_m \left(\frac{3}{4} l_B^2 \nabla_{[(r_1+r_3)/2-r_2]}^2 \right) \psi_{n_4}(r_3) \psi_{n_5}(r_2) \psi_{n_6}(r_1) \\ & \propto \sum_{\sigma} \int \frac{d^2 q d^2 p}{(2\pi)^4} \int \prod_i^3 d^2 r_i L_m \left(\frac{3}{4} (p-q)^2 l_B^2 \right) e^{iq \cdot (r_1-r_2)} e^{ip \cdot (r_2-r_3)} \psi_{n_1}^{\dagger}(r_1) \psi_{n_2}^{\dagger}(r_2) \psi_{n_3}^{\dagger}(r_3) \psi_{n_4}(r_3) \psi_{n_5}(r_2) \psi_{n_6}(r_1). \end{aligned} \quad (47)$$

The \sum_{σ} sum refers to a symmetric (antisymmetric) sum over all permutations σ assuming the particles are bosons (fermions). We have $k = q - p$ because

$$\begin{aligned} e^{iq \cdot (r_1-r_2)} e^{ip \cdot (r_2-r_3)} &= e^{i(q-p) \cdot ((r_1+r_3)/2-r_2)} e^{i(p+q) \cdot (r_1-r_3)/2} \\ &= e^{i(q-p) \cdot w_2} e^{i(p+q) \cdot w_3}, \end{aligned} \quad (48)$$

where w_2 and w_3 are linear combinations of the original coordinates whose roles will be further expounded in Appendix B. Here, it is sufficient to understand that k should be the momentum conjugate to w_2 , the total relative angular momentum. As before, $\psi_n(r) = \frac{1}{\sqrt{\sqrt{\pi} L l_B}} e^{i \frac{\kappa}{l_B} n y} e^{-\frac{(x - \kappa n l_B)^2}{2l_B^2}}$ and $\kappa = \frac{2\pi l_B}{L_y}$ is a dimensionless ratio that is small in the limit of large magnetic fields.

The integrals related to (47) can be simplified to a convenient form. As its computation is instructive for the generalization to more complicated cases, we explicate it in Appendix E. The 3-body bosonic PP U^0 which hosts the Pfaffian ground state is given by

$$U^0 \propto \sum_R \hat{b}_R^{\dagger} \hat{b}_R,$$

relative to the first one. Indeed, we see from Eq. 46 that w represents the relative separation between particle N and the CM of the rest of the particles. Note the appearance of the factor $\frac{N}{2(N-1)}$, which is essential in obtaining the correct expressions for the PPs. (It will be derived in detail in Appendix B.)

The next step is to express $U^m(k)$ in the LLL Landau gauge basis. Since the latter is the analogue of the Wannier basis, once we have done so, we are able to read off the Wannier basis matrix elements of a many-body FCI Hamiltonian exhibiting e.g. Pfaffian or other more exotic groundstates. Here we shall perform this explicitly for $N=3$ bosonic PPs. The computation with fermions or more bodies is conceptually similar. According to Eq. 45, we rescale the magnetic length l^2 by $\frac{3}{4} l^2$. Hence, U^m becomes $V_0 L_m(\frac{3}{4} k^2)$, where k is the momentum conjugate to the total relative coordinate $((r_1 - r_2) + (r_3 - r_2))/2$. In the basis of LLL Landau gauge eigenfunctions,

where

$$\begin{aligned} & \hat{b}_R \\ &= \sum_{n_i=3R \bmod N} \left[\sum_{s_i=0} e^{-\frac{\kappa^2}{2} \sum_i (R - (n_i + N s_i))^2} \right] c_{n_1} c_{n_2} c_{n_3} \\ &= \sum_{n_1+n_2+n_3=3R \bmod N} \left[\sum_{s,t} e^{-\frac{\kappa^2}{3} W_{st}} \right] c_{n_1} c_{n_2} c_{n_3}, \end{aligned} \quad (49)$$

with $W_{st} = \sum_i n_i'^2 - \sum_{i < j} n_i' n_j'$, $n_1' = n_1 + sN$, $n_2' = n_2 + tN$, and $n_3' = n_3 - N(s+t)$. The $N = L_x L_y$ periodicity originates from the properties of the Wannier basis on the torus. This result has been previously obtained in Ref. 55. However, the GHP formalism here can also generate higher PPs of multi-body interactions, and this result is just its simplest case. Note that the summation constraint $n_1 + n_2 + n_3 = 3R \bmod N$ can also be implemented as constraints over s, t , as in the 2-body case described in Ref. 43.

We see that U^0 is positive semidefinite. Since the Pfaffian state |Pf> resides in its kernel^{53,55}, we have

$$\langle \text{Pf} | U^0 | \text{Pf} \rangle = 0$$

as well as

$$b^R|\text{Pf}\rangle = 0.$$

As a consequence, the Pfaffian state is not just the ground state of U^0 but is also annihilated by all b_R 's. Analogous to the two-body case, U^0 consists of all three-body processes that conserve the CM R . The physical positions of the particles relative to their CM is described by $R - (n_i + Ns_i)$, where n_i is the real space basis index before enforcing the periodicity. When κ is suffi-

ciently small, contributions from periodic images can be discarded, and we are left with a simpler expression with $|R - (n_i + Ns_i)| < N = L_x L_y$.

Using our setup, we can likewise calculate higher PPs. U^1 vanishes due to the symmetric exchange statistics of the bosons. From Appendix E, we have

$$U^2 \propto \sum_R \hat{b}_R^\dagger \hat{b}_R,$$

where

$$\hat{b}_R = \sum_{n_1+n_2+n_3=3R \bmod N} \left[\sum_{s,t} \left(1 - \frac{2\kappa^2}{3} W_{st} \right) e^{-\frac{\kappa^2 W_{st}}{3}} \right] c_{n_1} c_{n_2} c_{n_3}, \quad (50)$$

with $W_{st} = \sum_i n'_i{}^2 - \sum_{i<j} n'_i n'_j$, $n'_1 = n_1 + sN$, $n'_2 = n_2 + tN$, and $n'_3 = n_3 - N(s+t)$ as before.

B. Discussion

While generic FCI models will only contain two-body interactions at the bare level, our many-body pseudopotentials will be useful for the construction of trial Hamiltonians which exhibit new exotic groundstates. This situation is similar for the FQHE case. There, the many-body PPs are primarily used to provide trial Hamiltonians for which various FQHE states are exact null modes. As stated before in Section III, the exact null mode property is tied to the clustering property which is enforced by the N -body trial Hamiltonian as N particles approach each other. This will be an interesting analogous application for the FCI scenario. By use of our many-body PPs, various trial states can be realized in a FCI model, including fractional Abelian states such as the Laughlin series, fractional non-Abelian states such as the Read-Rezayi series, but also even more exotic states such as a FCI Gaffnian state^{56–58}. For the Pfaffian FCI state, for example, it is interesting to study the interpolation of the exact FCI Hamiltonian to a generic FCI model and see whether adiabatic connectivity can be reached both at the level of Hamiltonians and entanglement spectra⁵⁰.

Many-body FCI pseudopotentials will also be useful in studying interactions beyond the effective single-band level. For instance, they are generically generated when interband scattering is considered. Moreover, following the construction introduced in Ref. 38 for the hardcore potential, we can map all these states to effectively one-dimensional models (see also Appendix B and E), and even higher dimensional generalizations⁵⁹, of featureless Mott insulators with exotic ground state and quasiparticle properties, which already are worth studying in their own right.

The use of many-body pseudopotential both as trial Hamiltonians and as effective Hamiltonians opens up new branches of research. For example, it will be interesting to apply the pseudopotential formalism to the model

discussed in the recent work Ref. 70, where convincing numerical evidence for a stable $\nu = 1$ non-Abelian state is presented. For our present work, we shall satisfy ourselves with developing the pseudopotential formalism.

VII. CONCLUSION

We have developed a pseudopotential formalism for fractional Chern insulators. Starting from the FCI Wannier state representation, we have employed the FQHE formalism on the cylinder and torus to define two-body as well as many-body PPs. We have decomposed bare FCI models into PPs and find that generic situations give rise to PP-decomposable and PP-nondecomposable parts of the FCI Hamiltonian, and discussed their interplay with partial breaking of magnetic translation group, which appears to be reemergent at low energies in the FCI models. We have defined many-body PPs to establish a basis for studying further unconventional FCI phases via appropriately designed trial Hamiltonians. We believe that it will be interesting to employ the PP perspective to provide a complementary tool to entanglement measures and to further develop our understanding of fractional Chern phases, as well as to extend its applicability to Chern bands of higher Chern number^{39,60–63} and two-dimensional fractional topological insulator models^{64–67}.

ACKNOWLEDGMENTS

We thank E. J. Bergholtz, C. Chamon, C. M. Jian, T. Neupert, Z. Papic, S. A. Parameswaran, A. Seidel, and D. N. Sheng for discussions. CH is supported by a scholarship from the Agency of Science, Technology and Research of Singapore. RT is supported by an SITP fellowship by Stanford University. XLQ is supported by the Packard foundation and the Alfred P. Sloan foundation.

Appendix A: Equivalence of the Landau-level-projected and Cartesian description on the cylinder

We reconcile the two expressions for the delta function potentials on the cylinder appearing in Refs. 38 and 42. The following arguments are valid for generic l_B , which has been set to unity in the following. We show that

$$\langle 0 | \delta^2(r - r') | 0 \rangle = e^{-(r_p - r'_p)^2/2}, \quad (\text{A1})$$

where $|0\rangle \sim f(z)e^{-|z|^2/4}$ denotes the LLL wavefunction and $r_p = (x_p, y_p)$ are the guiding-center coordinates defined by

$$\begin{aligned} x_p &=: \partial_z + \frac{z}{2} :, \\ y_p &=: -i\partial_z + \frac{iz}{2} : \end{aligned}$$

with $z = x - iy$. These are the LLL-projected coordinates since $z_p = z$, $\bar{z}_p =: 2\partial_z$ (see Ref. 68). Here, the normal-ordering symbols “:” indicate that any derivative within them does not act on the Gaussian factor $e^{-|z|^2/4}$ present

in LL wavefunctions. Note that $[x_p, y_p] = i$, i.e. the guiding-center coordinates do not commute. Consider a general interaction

$$V(r - r') = \int \frac{d^2k}{(2\pi)^2} V(k) e^{ik \cdot (r - r')}.$$

Let us project it onto the LLL $|0\rangle = f(z)e^{-|z|^2/4}$, i.e.

$$\langle 0 | V(r - r') | 0 \rangle = \int \frac{d^2k}{(2\pi)^2} V(k) \langle 0 | e^{ik \cdot (r - r')} | 0 \rangle.$$

The quantity in the angle brackets is evaluated as

$$\begin{aligned} \langle 0 | e^{ik \cdot r} | 0 \rangle &= \langle 0 | e^{i(k\bar{z} + \bar{k}z)/2} | 0 \rangle \\ &= \langle 0 | e^{\frac{i}{\sqrt{2}}(\bar{k}a + ka^\dagger)} e^{\frac{i}{\sqrt{2}}(\bar{k}b^\dagger + kb)} | 0 \rangle \\ &= e^{-|k|^2/2} \langle 0 | e^{\frac{i}{\sqrt{2}}(ka^\dagger)} e^{\frac{i}{\sqrt{2}}(\bar{k}a)} e^{\frac{i}{\sqrt{2}}(\bar{k}b^\dagger + kb)} | 0 \rangle \\ &= e^{-|k|^2/2} \langle 0 | e^{\frac{i}{\sqrt{2}}(\bar{k}b^\dagger + kb)} | 0 \rangle, \end{aligned} \quad (\text{A2})$$

where $k = k_x - ik_y$ and $a, b, a^\dagger, b^\dagger$ are lowering and raising operators of angular momentum and LL (see also Appendix B). Due to the specific form of $|0\rangle$, we also have

$$\begin{aligned} b|0\rangle &= \frac{1}{\sqrt{2}} \left(\frac{\bar{z}}{2} + 2\partial_z \right) f(z) e^{-|z|^2/4} = \frac{1}{\sqrt{2}} : 2\partial_z : f(z) e^{-|z|^2/4} = \frac{1}{\sqrt{2}} z_p |0\rangle, \\ b^\dagger|0\rangle &= \frac{1}{\sqrt{2}} \left(\frac{z}{2} - 2\partial_{\bar{z}} \right) f(z) e^{-|z|^2/4} = \frac{1}{\sqrt{2}} : z : f(z) e^{-|z|^2/4} = \frac{1}{\sqrt{2}} \bar{z}_p |0\rangle. \end{aligned} \quad (\text{A3})$$

Hence,

$$\begin{aligned} \langle 0 | e^{ik \cdot r} | 0 \rangle &= e^{-|k|^2/2} \langle 0 | e^{\frac{i}{2}(\bar{k}z_p + k\bar{z})} | 0 \rangle \\ &= e^{-|k|^2/2} \langle 0 | e^{ik \cdot r_p} | 0 \rangle. \end{aligned} \quad (\text{A4})$$

If we start from a delta function in real space, $V(k) = 1$, we obtain

$$\langle 0 | \delta^2(r - r') | 0 \rangle = \int \frac{d^2k}{(2\pi)^2} e^{-|k|^2/2} e^{ik \cdot r_p} = e^{-(r_p - r'_p)^2/2}.$$

Higher PPs in the LLL will thus be of the form $L_m(\nabla_p^2) e^{-(r_p - r'_p)^2/2}$. To summarize, the LLL projection leads to two types of modifications. Firstly, the delta function is replaced by a Gaussian in guiding-center coordinates. Secondly, the derivative will also be taken with respect to guiding-center coordinates.

Appendix B: First-principle derivation of Generalized Haldane Pseudopotentials

We generalize the Haldane pseudopotentials to $N > 2$ bodied interactions, i.e. GHPs, for fractionally filled

Chern bands. The main technical steps in this appendix include (i) a derivation of the GHP starting from an original interaction Hamiltonian involving arbitrarily many bodies (ii) a clarification on how the total relative angular momentum can be defined through an appropriate change of coordinates. The results of this appendix will be directly utilized in Appendix E for explicit calculations of the first 3-body PPs, which always take the factorized form $\sim \sum_n \hat{b}_n^\dagger \hat{b}_n$.

We start with the N -body Hamiltonian

$$\begin{aligned} H &= \frac{1}{2m} \sum_i^N (\vec{p}_i + \frac{e}{c} \vec{A}_i)^2 + V(\vec{x}_1, \vec{x}_2, \dots, \vec{x}_N) \\ &= \frac{1}{2m} \sum_i^N \left(-i \frac{\partial}{\partial x_i} - \frac{eB}{c} \frac{y_i}{2} \right)^2 + \left(-i \frac{\partial}{\partial y_i} + \frac{eB}{c} \frac{x_i}{2} \right)^2 \\ &\quad + V(\vec{x}_1, \vec{x}_2, \dots, \vec{x}_N) \\ &= \frac{1}{2m} \sum_i^N \left[-4l_B^2 \frac{\partial^2}{\partial z_i \partial \bar{z}_i} + \frac{1}{4l_B^2} |z_i|^2 + \left(\bar{z}_i \frac{\partial}{\partial \bar{z}_i} - z_i \frac{\partial}{\partial z_i} \right) \right] \\ &\quad + V(\vec{x}_1, \vec{x}_2, \dots, \vec{x}_N), \end{aligned} \quad (\text{B1})$$

where $z_i = x_i - iy_i$, $\vec{A}_i = B(-y_i, x_i, 0)/2$ and $l_B = \sqrt{\frac{\hbar c}{eB}}$.

The symmetric gauge has been used so that the Hamiltonian eigenstates will be conveniently labelled by angular momentum. However, the results that follow will be gauge-invariant. For now, we will not make any assumption about the form of the interaction potential V .

Haldane's original procedure was to first separate this Hamiltonian into a CM part and relative part, and then project the relative part into different angular momentum sectors²⁸. The same will be done here, but with N particles instead of two. Define a change of coordinate

$$w_i = R_{ij} z_j,$$

with $w_1 = (z_1 + z_2 + \dots + z_N)/N$, i.e. the CM coordinate. Any part of the resultant Hamiltonian depending only on w_1 will not affect our PP expansion.

1. Allowed coordinate transforms R_{ij}

It turns out that we are not free to choose the rest of R_{ij} arbitrarily. If we want to have a well-defined angular momentum decomposition in terms of the new variables $\{w_i\}$, we will need to ensure that the resultant Hamiltonian is of the same form as the last line of Eq. B1. This is because the kinetic term in (B1) can be written as

$$\begin{aligned} H_{kin} &= \frac{1}{2m} \sum_i^N \left[-4l_B^2 \frac{\partial^2}{\partial z_i \partial \bar{z}_i} + \frac{1}{4l_B^2} |z_i|^2 + (\bar{z}_i \frac{\partial}{\partial \bar{z}_i} - z_i \frac{\partial}{\partial z_i}) \right] \\ &= \hbar\omega \sum_i (b_i^\dagger b_i + \frac{1}{2}) + \hbar\omega (a_i^\dagger a_i - b_i^\dagger b_i) \\ &= \hbar\omega \sum_i (a_i^\dagger a_i + \frac{1}{2}), \end{aligned} \quad (\text{B2})$$

with eigenstates labeled by angular momentum m and LL index n :

$$|n, m\rangle = \frac{(b^\dagger)^{m+n} (a^\dagger)^n}{\sqrt{(m+n)!} \sqrt{n!}} |0, 0\rangle. \quad (\text{B3})$$

This can be seen from how the angular momentum operator exist as part of the kinetic single-particle Hamiltonian. With the second-quantized operators defined by (particle index i suppressed)

$$a = \frac{1}{\sqrt{2}} \left(\frac{z}{2l_B} + 2l_B \frac{\partial}{\partial \bar{z}} \right),$$

$$b = \frac{1}{\sqrt{2}} \left(\frac{\bar{z}}{2l_B} + 2l_B \frac{\partial}{\partial z} \right),$$

the angular momentum operator is

$$L = \hbar \left(\bar{z} \frac{\partial}{\partial \bar{z}} - z \frac{\partial}{\partial z} \right) = \hbar (a^\dagger a - b^\dagger b).$$

To expand in terms of angular momentum eigenstates, the coordinate transform R_{ij} must leave the form of each

term of the last line of Eq. B1 invariant, i.e. $|z_i|^2$ must transform into a sum of similar quadratic terms, etc.

Denoting $z = (z_1, z_2, \dots, z_N)^T$, $\partial z = (\frac{\partial}{\partial z_1}, \frac{\partial}{\partial z_2}, \dots, \frac{\partial}{\partial z_N})^T$, and likewise for the w 's, the various terms transform as

$$\sum_i \frac{\partial^2}{\partial z_i \partial \bar{z}_i} = \partial \bar{z}^T \partial z = \partial \bar{w}^T [RR^T] \partial w, \quad (\text{B4})$$

$$\sum_i |z_i|^2 = \bar{z}^T z = \bar{w}^T [(R^{-1})^T (R^{-1})] w = \bar{w}^T [RR^T]^{-1} w, \quad (\text{B5})$$

$$\sum_i z_i \frac{\partial}{\partial z_i} = z^T \partial z = w^T [(R^{-1})^T R^T] \partial w = w^T \partial w. \quad (\text{B6})$$

The Hamiltonian retains the same form if RR^T is diagonal. If we regard R as a rotation matrix, we see that this condition is satisfied whenever R maps an orthogonal basis to another orthogonal basis. Hence an allowed R consists of mutually orthogonal rows. As a simple example, the R matrix for 2 particles satisfies the condition

$$\begin{pmatrix} 1/2 & 1/2 \\ 1 & -1 \end{pmatrix},$$

according to the CM coordinate $w_1 = (z_1 + z_2)/2$ and the relative coordinate $w_2 = z_2 - z_1$.

2. The explicit form of the Hamiltonian transformed into total relative coordinates

The next step is to explicitly find the coefficients of the transformed Hamiltonian. Since we are interested in a PP expansion in the total angular momentum, we define the total relative coordinate

$$w_2 = \frac{1}{N-1} \sum_{n=1}^{N-1} (z_n - z_N) = \frac{\sum_i^{N-1} z_i}{N-1} - z_N. \quad (\text{B7})$$

The other coordinates can be arbitrarily defined as long as they are orthogonal to w_2 and $w_1 = \frac{1}{N} \sum_i^N z_i$. With this choice, the diagonal elements of RR^T are

$$\lambda_1 = N, \lambda_2 = \frac{N}{N-1}, \dots$$

Hence the kinetic part of the Hamiltonian becomes

$$\begin{aligned} H_{kin} &= \frac{1}{2m} \sum_i^N \left[-4l_B^2 \lambda_i \frac{\partial^2}{\partial w_i \partial \bar{w}_i} + \frac{1}{4l_B^2 \lambda_i} |w_i|^2 \right. \\ &\quad \left. + (\bar{w}_i \frac{\partial}{\partial \bar{w}_i} - w_i \frac{\partial}{\partial w_i}) \right] \\ &= \frac{1}{2m} \left[-4l_{rel}^2 \frac{\partial^2}{\partial w_2 \partial \bar{w}_2} + \frac{1}{4l_{rel}^2} |w_2|^2 \right. \\ &\quad \left. + (\bar{w}_2 \frac{\partial}{\partial \bar{w}_2} - w_2 \frac{\partial}{\partial w_2}) \right] + \dots, \end{aligned} \quad (\text{B8})$$

where $l_{\text{rel}} = l_B \sqrt{\lambda_2} = l_B \sqrt{\frac{N}{N-1}}$ is the effective "magnetic length" for the total relative coordinate. Only the terms corresponding to the total relative coordinate are shown in the second line. In general, the diagonal elements of RR^T $\lambda_1, \lambda_2, \lambda_3, \dots, \lambda_N$ define a set of effective magnetic lengths $l_i = l_B \sqrt{\lambda_i}$.

3. Derivation of the N-body pseudopotential

We are now set up to find $\langle m_1, \dots, m_N | V | m_1, \dots, m_N \rangle$, the projection of an interaction potential $V(w_1, w_2, \dots, w_N)$ onto the angular momentum sector in the LLL. This projection is of course dependent on $w = Rz$. For the w_1 and w_2 previously defined as the CM and total relative coordinates, m_1 and m_2 correspond to the CM angular momentum and total relative angular momentum, respectively. To evaluate this matrix element, we Fourier transform to shift the coordinate dependencies onto an universal exponential factor:

$$\begin{aligned}
V^{m_1 m_2 \dots m_N} &= (4\pi)^N \langle m_1, \dots, m_N | V(w_1, \dots, w_N) | m_1, \dots, m_N \rangle \\
&= (4\pi)^N \langle m_1, \dots, m_N | \left(\prod_j^N \int \frac{d^2(k_j l_j)}{(2\pi)^2} \right) V(k_1, \dots, k_N) \prod_j^N e^{ik_j \cdot w_j} | m_1, \dots, m_N \rangle \\
&= (4\pi)^N \left(\prod_j^N \int \frac{d^2(k_j l_j)}{(2\pi)^2} \right) \prod_j^N \langle m_j | V(k_1, \dots, k_N) e^{ik_j \cdot w_j} | m_j \rangle \\
&= (4\pi)^N \left(\prod_j^N \int \frac{d^2(k_j l_j)}{(2\pi)^2} \right) V(k_1, \dots, k_N) \prod_j^N \langle m_j | e^{ik_j \cdot w_j} | m_j \rangle. \tag{B9}
\end{aligned}$$

The momentum-space potential V in the last line can be taken out of the expectation value since the momenta labeled by k_j s are regarded as complex numbers. For each j ,

$$\begin{aligned}
\langle m_j | e^{ik \cdot w_j} | m_j \rangle &= \langle m_j | e^{i \frac{l_j}{2} (k \bar{z} + \bar{k} z)} | m_j \rangle = \langle m_j | e^{\frac{i l_j}{\sqrt{2}} (\bar{k} a_j + k a_j^\dagger)} e^{\frac{i l_j}{\sqrt{2}} (\bar{k} b_j^\dagger + k b_j)} | m_j \rangle \\
&= e^{-|k|^2 l_j^2 / 4} \langle m_j | e^{i \frac{l_j}{\sqrt{2}} k a_j^\dagger} e^{i \frac{l_j}{\sqrt{2}} \bar{k} a_j} e^{i \frac{l_j}{\sqrt{2}} (\bar{k} b_j^\dagger + k b_j)} | m_j \rangle = e^{-|k|^2 l_j^2 / 2} \langle m_j | e^{\frac{i l_j}{\sqrt{2}} \bar{k} b_j^\dagger} e^{\frac{i l_j}{\sqrt{2}} k b_j} | m_j \rangle \\
&= e^{-|k|^2 l_j^2 / 2} \sum_{s=0}^{\infty} \frac{1}{(s!)^2} \langle m_j | \left(\frac{i l_j \bar{k} b_j^\dagger}{\sqrt{2}} \right)^s \left(\frac{i l_j k b_j}{\sqrt{2}} \right)^s | m_j \rangle = e^{-|k|^2 l_j^2 / 2} \sum_{s=0}^{\infty} \frac{m!}{(s!)^2 (m-s)!} \left(\frac{-l_j^2 |k|^2}{2} \right)^s \\
&= e^{-|k|^2 l_j^2 / 2} L_m \left(\frac{l_j^2 |k|^2}{2} \right). \tag{B10}
\end{aligned}$$

The terms containing the a_j and a_j^\dagger operators in the third line reduce to unity because the states are already defined to be in the LLL. Use has been made of the Baker-Campbell-Hausdorff formula in producing the factors of $e^{-|k|^2 l_j^2 / 4}$.

The LLL projected pseudopotential component reads

$$\begin{aligned}
&V^{m_1 m_2 \dots m_N} \\
&= \langle m_1, \dots, m_N | V(w_1, w_2, \dots, w_N) | m_1, \dots, m_N \rangle \\
&= \prod_j^N \int \frac{d^2(k_j l_j)}{\pi} e^{-|k_j|^2 l_j^2 / 2} L_{m_j} \left(\frac{l_j^2 |k_j|^2}{2} \right) V(k_1, \dots, k_N), \tag{B11}
\end{aligned}$$

where $V(k_1, \dots, k_N)$ is the Fourier transform of $V(w_1, \dots, w_N)$. We focus on the w_2 degree of freedom. Let $|m\rangle$ denote the state where $m_2 = m$ and all other $m_i = 0$, i.e. the state with total relative angular momen-

tum m . Then the m th PP component for a translationally invariant interaction is

$$\begin{aligned}
V^m &= \left(\prod_{j=2}^N \int \frac{d^2(k_j l_j)}{\pi} e^{-|k_j|^2 l_j^2 / 2} \right) \\
&\quad \times L_m \left(\frac{N l_B^2 |k_j|^2}{2(N-1)} \right) V(k_2, k_3, \dots, k_N). \tag{B12}
\end{aligned}$$

The integral over k_1 has been omitted since V does not depend on the CM coordinate w_1 . Also, the rest of the Laguerre polynomial factors have disappeared since $L_0 = 1$. We still need to define $V^{m_2 \dots m_N}(k_2, k_3, \dots, k_N)$ such

that it corresponds to a PP component

$$\langle m_1, \dots, m_N | V(w_1, w_2, \dots, w_N) | m_1, \dots, m_N \rangle$$

that is nonzero only at the simultaneous set of angular momenta m_2, \dots, m_N . This is done by exploiting the orthonormality relation $\int_0^\infty 2qe^{-q^2} L_s(q^2) L_t(q^2) dq = \delta_{st}$. Switching to polar coordinates, we see that the functional form of the pseudopotential is given by

$$U^{m_2, \dots, m_N} = V_0 \prod_{j=2}^N L_{m_j} \left(\frac{k_j^2 l_j^2}{2} \right), \quad (\text{B13})$$

where V_0 is again a constant with units of energy. If we want a PP that has no angular momentum on the spurious degrees of freedom w_3, w_4, \dots , we find

$$U^m(k) = V_0 L_m \left(\frac{k^2 l_B^2 N}{2(N-1)} \right). \quad (\text{B14})$$

This reproduces the familiar result $U^m(k) = L_m(k^2 l_B^2)$ for $N = 2$. For $N = 3$, $U^m(k) = L_m(\frac{3}{4} k^2 l_B^2)$ where m is the total relative angular momentum characterized by $w_2 = \frac{1}{2}((z_1 - z_3) + (z_2 - z_3))$. The latter will be used extensively in the calculations of the next section.

4. Discussion and Generalizations

We can determine how the effective magnetic length l_j should be rescaled without assuming the explicit form w_j defined in terms of the z_i s. By examining the diagonal elements of RR^T , we find that

$$l_i = l_B \sqrt{\sum_j^{N-1} R_{ij}^2 + \sum_{j < k}^{N-1} R_{ij} R_{ik}}$$

$$V_{n'_1 \dots n'_N; n_1 \dots n_N}^{m_1 m_2 \dots m_N} = \langle n'_1, \dots, n'_N; m_1, \dots, m_N | V(w_1, w_2, \dots, w_N) | n_1, \dots, n_N; m_1, \dots, m_N \rangle =$$

$$\left(\prod_j^N \int \frac{d^2(k_j l_j)}{\pi} e^{-|k_j|^2 l_j^2 / 2} L_{m_j} \left(\frac{l_j^2 |k_j|^2}{2} \right) \right) \prod_i^N \left(\frac{-il_B(R_{li} k_l)}{\sqrt{2}} \right)^{n'_i - n_i} \sqrt{\frac{n_i!}{n'_i!}} L_{n'_i - n_i} \left(\frac{l_B^2 |(R_{li} k_l)|^2}{2} \right) V(k_1, \dots, k_N), \quad (\text{B15})$$

with the effective magnetic lengths l_j as before.

If V is translationally invariant, it does not depend on $w_1 = (z_1 + \dots + z_N)/N$, and the k_1 integral produces a delta function $\delta(k_1)$. Hence, as is usually the case, k_1 should be excluded from all sums in Eq. B15. As an illustration for $N = 2$ bodies with interaction independent of the CM, only the k_2 integration survives. We have

$$V_{n_1 n_2; n_1 n_2}^{m_2} \propto \int d^2 k e^{-l_B^2 k^2} L_m(l_B^2 k^2) L_{n_1} \left(\frac{l_B^2 k^2}{2} \right) L_{n_2} \left(\frac{l_B^2 k^2}{2} \right) V(k_2). \quad (\text{B16})$$

for $i > 1$. For $i = 1$, $l_1 = \sqrt{N} l_B$. Here, w_1 is the CM position and l_1 is the effective magnetic length for the CM angular momentum.

(B11) can also be extended to cases beyond the LLL. There, the a and a^\dagger terms in the third line of Eq. B10 will not yield unity. If we consider the case where each particle occupies a specific Landau Level, we will have to first calculate expressions such as $e^{i \frac{l_j}{\sqrt{2}} k a_j^\dagger} e^{i \frac{l_j}{\sqrt{2}} \bar{k} a_j}$ before making the change of coordinates from z to w . This is because the positions of the particles are indexed by z , not w .

To begin with, we rearrange the exponential factor in the Fourier transform $e^{ik_j \cdot w_j} = e^{i(k_j R_{ji}) z_i}$ so that it depends explicitly on the z_i s, albeit with modified $k = (k_j R_{ji})$, summation implied. After some algebra, we find

$$\langle n' | e^{i \frac{l_j}{\sqrt{2}} k a_j^\dagger} e^{i \frac{l_j}{\sqrt{2}} \bar{k} a_j} | n \rangle = \left(-\frac{il_B k}{\sqrt{2}} \right)^{n' - n} \sqrt{\frac{n!}{n'!}} L_{n' - n} \left(\frac{l_B^2 |k|^2}{2} \right),$$

where n and n' denote the initial and final Landau levels of the particle. When $n = n'$, we just have $L_n(k^2 l_B^2 / 2)$. With the states being reduced to the LLL, we proceed as in (B11), arriving at the general formula for the PP between N particles initially at LLs n_1, n_2, \dots, n_N mapping to LLs n'_1, n'_2, \dots, n'_N , with angular momenta m_1, m_2, \dots, m_N associated with the coordinates $w_i = R_{ij} z_j$:

$R_{li} k_l = \pm k_2$ and $V = V(k_2)$. m_1 , the CM angular momentum, is irrelevant for the interaction, so $V_{m_1} = \delta_{m_1, 0}$. We can also deduce this result from the orthogonality of the Laguerre polynomials: if we impose the further restriction $n_i = n'_i$ for all i , i.e. particles stay in their respective LLs, Eq. B15 reduces to

Appendix C: Derivation of 2-body Pseudopotential Hamiltonians on a Cylinder

Here, we present the details of the derivation of the two-body PPs U^m . We shall explicitly work through only the fermionic case, since the bosonic case can be analogously derived. From Eq. 21, a special case of Eq. B16, the potential U^m that is nonzero only for

$$\begin{aligned} U_{n_1 n_2 n_3 n_4}^m &= \frac{V_0}{4} \int d^2 r d^2 r' \psi_{n_1}^\dagger(r) \psi_{n_2}^\dagger(r') L_m(-l_B^2 \nabla^2) \delta^2(r-r') \psi_{n_3}(r') \psi_{n_4}(r) + \text{antisymm} \\ &= \frac{V_0}{4} \int \frac{l_B^2 d^2 q}{(2\pi)^2} \int d^2 r d^2 r' L_m(q^2 l_B^2) e^{iq \cdot (r-r')} \psi_{n_1}^\dagger(r) \psi_{n_2}^\dagger(r') \psi_{n_3}(r') \psi_{n_4}(r) + \text{antisymm}. \end{aligned} \quad (\text{C1})$$

Recall that $\kappa = \frac{2\pi l_B}{L_y}$ is a dimensionless ratio that is small in the limit of large magnetic fields. The two types of MT symmetry constraints mentioned in Section V are manifest in the above expression as (i) the CM conservation which corresponds to $n_1 + n_2 = n_3 + n_4$, and (ii) one-dimensional translation symmetry, which is the invariance of U^m under $n_i \rightarrow n_i + a$, where a is an integer and $i = 1, 2, 3, 4$. (A similar observation has been independently made in Ref. 27.) CM conservation must be present because the $\int dy$ and $\int dy'$ integrals produce delta functions of the form

$$\delta\left(\frac{2\pi}{L_y}(n_4 - n_1) + q_y\right)$$

$$\begin{aligned} U_{l_1 l_2}^m &= \frac{V_0}{4\pi L_y^2 l_B^4} \frac{L_y}{2\pi} \pi l_B^2 \int d^2 q \delta(q_y + \frac{2\pi}{L_y}(l_1 - l_2)) L_m(l_B^2 q^2) e^{-\frac{l_B^2 q_x^2}{2}} e^{i\kappa l_B(l_1+l_2)q_x} e^{-\frac{\kappa^2(l_1-l_2)^2}{2}} + \text{antisymm} \\ &= \frac{V_0}{4\pi L_y^2 l_B^2} \frac{L_y}{2\pi} \pi l_B^2 \int d^2 q \delta(q_y + \frac{2\pi}{L_y}(l_1 - l_2)) L_m(l_B^2 q^2) e^{-\frac{l_B^2 q^2}{2}} e^{i\kappa l_B(l_1+l_2)q_x} + \text{antisymm}. \end{aligned} \quad (\text{C2})$$

The second line follows from the fact that q_y is constrained to be $q_y = \frac{2\pi}{L_y}(l_2 - l_1) = \frac{\kappa}{l_B}(l_2 - l_1)$. Note that n completely disappears from the expression, as expected from MT symmetry. A closed form expression for U^m is given by

$$\begin{aligned} U_{l_1 l_2}^m &= \\ g \kappa^3 \sum_{p=0}^m \frac{(-1)^{p+1} m!}{p!(m-p)!} \sum_{j=0}^p \sum_{r=0}^{j/2} \frac{\Gamma(p-j+r+1/2) 2^{m+j-r-3} (i\kappa)^{2(j-r-1)}}{(p-j)!(2r)!(j-2r)!\sqrt{\pi}(l_1 l_2)^{2r-j}} \left[(l_1 + l_2)^{2r} - (-1)^j (l_1 - l_2)^{2r} \right] e^{-\kappa^2(l_1^2 + l_2^2)}. \end{aligned} \quad (\text{C3})$$

The lengthy expression above can be factorized into the form $U_{l_1 l_2}^m = g \kappa^3 b_{l_1}^m b_{l_2}^m$, $g = 4V_0(2\pi)^{3/2}$, where

$$b_l^{2j+1} = l e^{-\kappa^2 l^2} \sum_{p=0}^j \frac{(-2)^{3p-j} (\kappa l)^{2p} \sqrt{(2j+1)!}}{(j-p)!(2p+1)!}. \quad (\text{C4})$$

the relative angular momentum sector m is given by $U^m(r-r') = V_0 L_m(-l_B^2 \nabla^2) \delta^2(r-r')$, where V_0 is a constant with units of energy. We find its LLL Landau gauge basis matrix elements $U_{n_1 n_2 n_3 n_4}^m$ by projecting onto the basis wavefunctions $\psi_n(r) = \frac{1}{\sqrt{\sqrt{\pi} L_y l_B}} e^{i \frac{\kappa}{l_B} n y} e^{-\frac{(x - \kappa n l_B)^2}{2 l_B^2}}$, where L_y is the circumference of the cylinder:

and

$$\delta\left(\frac{2\pi}{L_y}(n_3 - n_2) - q_y\right).$$

The CM conservation condition $n_1 + n_2 = n_3 + n_4$, i.e. $n = n'$, appears after we combine these two delta functions. Since the CM of each LLL wavefunction occurs along $x = \kappa l_B n \propto n$, we see that the CM of the particles must indeed be equal before and after a two-body hopping.

We explicitly resolve the MT symmetry via the translation $n_i \rightarrow n_i + 1$, as Fourier terms cancel upon $\psi_i(r) \rightarrow \psi_i\left(r - \frac{2\pi l_B^2}{L_y}\right)$. This is exactly a magnetic translation under which the system in a magnetic field $B = \frac{\hbar c}{e l_B^2}$ is expected to be invariant. To continue the calculation, reduce U^m to the $\int d^2 q$ integral

This result can be proven by induction. The first few b_l^{2j+1} s are

$$b_l^1 = l e^{-\kappa^2 l^2},$$

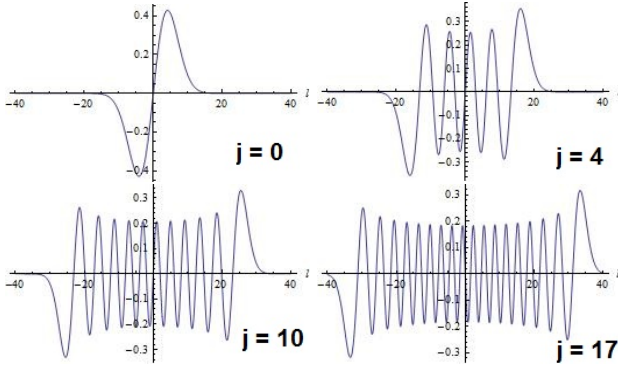


FIG. 9. Graphs of b^{2j+1} from Eq. C4 for $j = 0, 4, 10, 17$ with $\kappa = \frac{1}{6}$. As j increases, the main region of contribution of b^{2j+1} shifts in the direction of larger $|l|$.

$$b_l^3 = \frac{1}{\sqrt{3!}}(-3 + 4\kappa^2 l^2)l e^{-\kappa^2 l^2},$$

$$b_l^5 = \frac{1}{\sqrt{5!}}(15 - 40\kappa^2 l^2 + 16\kappa^4 l^4)l e^{-\kappa^2 l^2},$$

$$b_l^7 = \frac{1}{\sqrt{7!}}(-105 + 420\kappa^2 l^2 - 336\kappa^4 l^4 + 64\kappa^6 l^6)l e^{-\kappa^2 l^2},$$

$$b_l^{2j} = 0.$$

Certain b 's are depicted in Fig. 9 for illustration. Note that the U^m operators can always be decomposed into the product of two b^m operators that are m degree polynomials of l_1 and l_2 . These polynomials have the physically relevant property that (i) the b_l^m of higher m are "localized" at larger values of l and (ii) that they are orthogonal in the limit of $\kappa \rightarrow 0$ before we enforce the $L_x L_y$ periodicity in the x -direction of the cylinder. This is further explained in Appendix D.

We can similarly calculate the bosonic PPs through Eq. C2, but with terms symmetrized instead of anti-symmetrized over l_1 and l_2 . As before, the PPs can be written as $U_{l_1 l_2}^m = g \kappa^3 c_{l_1}^m c_{l_2}^m$, $g = 4V_0(2\pi)^{3/2}$, but now with the c^m 's taking the form

$$c_l^0 = e^{-\kappa^2 l^2},$$

$$c_l^2 = \frac{1}{\sqrt{2!}}(-1 + 4\kappa^2 l^2)l e^{-\kappa^2 l^2},$$

$$c_l^4 = \frac{1}{\sqrt{4!}}(3 - 24\kappa^2 l^2 + 16\kappa^4 l^4)l e^{-\kappa^2 l^2},$$

$$c_l^6 = \frac{1}{\sqrt{6!}}(-15 + 180\kappa^2 l^2 - 240\kappa^4 l^4 + 64\kappa^6 l^6)l e^{-\kappa^2 l^2},$$

$$c_l^{2j+1} = 0.$$

Note that both the bosonic and fermionic results can also be obtained via Gram-Schmidt Orthogonalization of the basis set comprising of even(odd) powers of κl with the inner product measure $e^{-2\kappa^2 l^2}$. Indeed, the functional forms of their polynomial part can be uniquely determined by orthonormality requirements once we have obtained the form of their inner product measure in Eq. C4.

Appendix D: Orthogonality of U^m

The FQH PPs U^m are not systematically orthogonal once we place them on a cylinder or torus. We will study the physical origin of this fact and make quantitative estimates in this appendix. While we are only concerned with quadratic cases of $L_x = L_y$ in this paper, it will be instructive to investigate how deviations from orthogonality depend on general L_x and L_y .

1. From plane to cylinder

When we compactify the plane into a cylinder, the notion of relative angular momentum is no longer well-defined. In a fixed LL, the relative angular momentum is proportional to the interparticle distance which can only be meaningfully defined when the latter is much smaller than L_y . Recall that the effective $\kappa = \frac{2\pi l_B}{L_y} = \frac{1}{L_y}$ after mapping to the FCI system. We thus expect orthogonality to occur only in the limit of large L_y , or, equivalently, small κ . To proceed, we evaluate the overlap elements of two PPs V_{cyl}^m and V_{cyl}^n , and show that the latter are orthogonal for sufficiently small κ .

$$\begin{aligned}
\langle U_{\text{cyl}}^m, U_{\text{cyl}}^n \rangle &\propto \sum_{l_1 l_2} U_{\text{cyl } l_1, l_2}^m U_{\text{cyl } l_1, l_2}^n \\
&\propto \sum_{l_1 l_2} \int d^2 q \int d^2 q' \delta(q_y + \frac{2\pi}{L_y}(l_1 - l_2)) \delta(q'_y - q_y) L_m(l_B^2 q^2) L_n(l_B^2 q'^2) e^{-\frac{l_B^2(q^2 + q'^2)}{2}} e^{i\kappa l_B(l_1 + l_2)(q_x + q'_x)} \\
&\propto \sum_{l_1 + l_2, l_1 - l_2} \int dq_y \int dq_x \int dq'_x \delta(q_y + \frac{2\pi}{L_y}(l_1 - l_2)) L_m(l_B^2 q^2) L_n(l_B^2 q'^2) e^{-\frac{l_B^2(q^2 + q'^2)}{2}} e^{i\kappa l_B(l_1 + l_2)(q_x + q'_x)} \\
&\propto \sum_{l_1 - l_2} \int dq_y \int dq_x \int dq'_x \delta(q_y + \frac{2\pi}{L_y}(l_1 - l_2)) L_m(l_B^2 q^2) L_n(l_B^2 q'^2) e^{-l_B^2 q^2} \delta(q_x + q'_x) \\
&\propto \int d^2 q \left(\sum_{l_1 - l_2} \delta(q_y + \frac{2\pi}{L_y}(l_1 - l_2)) \right) L_m(l_B^2 q^2) L_n(l_B^2 q^2) e^{-l_B^2 q^2} \\
&\approx \pi \int 2(q l_B) d(q l_B) \left(\sum_{l_1 - l_2} \delta((q_y l_B) + \kappa(l_1 - l_2)) \right) L_m(l_B^2 q^2) L_n(l_B^2 q^2) e^{-l_B^2 q^2} \\
&\rightarrow \pi \delta_{mn}.
\end{aligned} \tag{D1}$$

Two approximations have been made above. From the third last to second last line, we replace the non-rotationally invariant integral over $\int dq_x dq_y$ by the rotationally invariant integral $\pi \int 2qdq$. From the second last to the last line, the delta function sum in the large parentheses was replaced by unity, i.e. taking the limit where the range of $l_1 - l_2$ (and hence q) tends to infinity. These approximations become exact when the discrete $q_y l_B$ becomes a continuum, which occurs precisely when $\kappa \rightarrow 0$. Indeed, this agrees with the physical intuition that the relative angular momentum becomes a well-defined quantity when L_y is large. From the viewpoint of polynomial orthogonality, we see that the orthogonality of the U_{cyl}^m is respected as much as as the integral over Laguerre polynomials is allowed to be made continuous. Specifically, the orthogonality of the Laguerre polynomials is exact only for the continuum $q^2 = q_x^2 + q_y^2$ and not for discrete points specified by $\Delta l = l_1 - l_2$ whose separations do not vanish unless $\kappa = 0$.

2. From cylinder to torus

The compactification of the cylinder into a torus introduces a periodicity in the L_x -direction. This introduces periodic copies of U_{cyl}^m in U_{tor}^m , each displaced from another by $(L_x L_y, L_x L_y)$ or $(L_x L_y, -L_x L_y)$ sites in $l_1 - l_2$ space. Nonorthogonality is expected when there is significant overlap between these images. Let us obtain a bound by finding the conditions where $|U_{\text{cyl}}^m|$, whose explicit form is given by (C4), is not negligible, with l_1, l_2 being of the order of $L_x L_y$. At such values,

$$\begin{aligned}
U_{\text{cyl } l_1 l_2}^m &\sim e^{-2(\kappa L_x L_y)^2} (2^{3/2} \kappa L_x L_y)^{2m} \\
&= e^{-2w^2} (2^{3/2} w)^{2m} \\
&= f(w),
\end{aligned} \tag{D2}$$

where $w = \kappa L_x L_y$. The function $f(w)$ exhibits a rapid Gaussian decay beyond $w \approx 2\sqrt{m}$. Hence we expect the PP U^m to be nonorthogonal when

$$\kappa < \frac{2\sqrt{m}}{L_x L_y},$$

which implies that

$$L_x < 2\sqrt{m}, \tag{D3}$$

a bound well-verified by calculations in the following subsection.

3. Numerical results for the orthonormality of the fermionic pseudopotentials

The orthonormality of the U^m s can be studied quantitatively through their overlap matrix defined by

$$M_{mn} = \langle U^m, U^n \rangle \tag{D4}$$

according to Eq. 38. When the U^m s are orthonormal, it holds $M_{mn} = \mathbb{I}$. If the U^m s are not orthonormal while they span an orthonormal basis, the eigenvalues of M_{mn} will still be unity since we can find a unitary transformation where M_{mn} is diagonal. When U^m s are overcomplete, however, the spectrum of M broadens and yields eigenvalues deviating from this limit. In Fig. 10, we plot the eigenvalues of the overlap matrix for the first few PPs as a function of L . Orthogonality is hence broken when the eigenvalues differ from unity. Indeed, we observe that orthogonality improves with system size, in agreement with the conclusions of the preceding subsections.

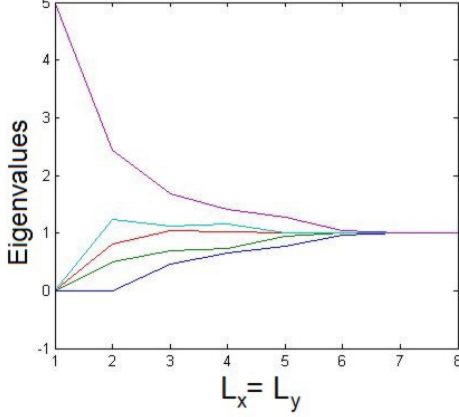


FIG. 10. (Color online) The eigenvalues of the overlap matrix of U^1, U^3, U^5, U^7 and U^9 as a function of the system size $L = L_x = L_y$. Indeed, we observe orthogonality when $L \geq 6$, in excellent agreement with the bound $2\sqrt{9} = 6$ from Eq. D3.

Appendix E: Three-body bosonic Pseudopotential calculations in the LLL Landau gauge basis

Let U^m be the bosonic 3-body CM-invariant potential which is nonzero only in the sector of total relative angular momentum m . Such 3-body U^m s will be useful as a basis through which arbitrary CM conserving potentials can be expanded. In this appendix, we will show the detailed derivation of U^m in the basis of LLL Landau gauge eigenfunctions, starting from Eq. C1.

According to Eq. B14, we have to replace the magnetic length l_B^2 by $\frac{3}{4}l_B^2$. This, however, causes no difference when $m = 0$, since $L_0 = 1$, so the results in Refs. 38 and 55 for U^0 could have been obtained without this modification along our GHPs.

After performing the $\int d^2r_i$ integrations according to Eq. C1, we arrive at

$$U_{n_1 n_2 n_3 n_4 n_5 n_6}^m \propto \sum_{\sigma} \int \frac{d^2q d^2p}{(2\pi)^4} I(q, n_1, n_6) I(p - q, n_2, n_5) I(-p, n_3, n_4) L_m \left(\frac{3}{4}(p - q)^2 l_B^2 \right), \quad (\text{E1})$$

where

$$I(q, n, n') = 2\pi \delta \left(q_y + \frac{\kappa}{l_B}(n - n') \right) e^{-l_B^2 q_x^2 / 4} e^{i\kappa l_B (n + n') q_x / 2} e^{-\kappa^2 (n - n')^2 / 4}.$$

Here, $\sum_{\sigma} = \frac{1}{(3!)^2} \sum_{perm(n_1 n_2 n_3)} \text{sgn}(perm)^f \sum_{perm(n_6 n_5 n_4)} \text{sgn}(perm)^f$ where $f = 1$ for fermions and $f = 0$ for bosons. $perm$ refers to the permutations of the n_i s while $\text{sgn}(perm) = \pm 1$ depending on whether the permutation is even or odd. Up to now, the expression is easily generalizable to any number of fermions or bosons by increasing the number of integrals and $I(q, n, n')$ s. If we further restrict ourselves to the 3-body bosonic case, we can simplify it to

$$\begin{aligned} & U_{n_1 n_2 n_3 n_4 n_5 n_6}^m \\ & \propto e^{-\kappa^2 [(n_1 - n_6)^2 + (n_2 - n_5)^2 + (n_3 - n_4)^2] / 4} \sum_{\sigma} \int \frac{d^2q_x d^2p_x}{(2\pi)^4} L_m \left(\frac{3}{4}(p - q)^2 l_B^2 \right) e^{-l_B^2 (p^2 + q^2 + (p - q)^2) / 4} e^{i\kappa l_B N_1 q / 2} e^{i\kappa l_B N_2 p / 2} \\ & \propto \sum_{\sigma} P_m(n_1, n_2, n_3, n_4, n_5, n_6; \kappa^2) \frac{4\pi}{\sqrt{3}} e^{-\frac{\kappa^2}{6}(N_1^2 + N_1 N_2 + N_2^2)}, \end{aligned} \quad (\text{E2})$$

where $N_1 = n_1 + n_6 - n_2 - n_5$, $N_2 = n_2 + n_5 - n_3 - n_4$. $P_m(n_1, n_2, n_3, n_4, n_5, n_6; \kappa^2)$ is a potentially complicated polynomial whose form depends on m . We define the conserved CM "Landau level wavefunction index" R via $3R \bmod N = n_1 + n_2 + n_3 = n_6 + n_5 + n_4$. The existence of R is a consequence of the total CM conservation of U^m .

1. $m=0$ for bosons on a torus

In this case, $L_0 = 1$, and $P_0(n_1, n_2, n_3, n_4, n_5, n_6; \kappa^2) = 1$. Since each of the n_i 's is also defined modulo N (but constrained to sum to $3R$ as shown above), we make the

replacement

$$\begin{aligned} & e^{-\frac{\kappa^2}{2}((R - n_1)^2 + (R - n_2)^2 + (R - n_3)^2)} \rightarrow \\ & \sum_{s, t} e^{-\frac{\kappa^2}{2}((R - (n_1 + Ns))^2 + (R - (n_2 + Nt))^2 + (R - (n_3 - N(t+s)))^2)}, \end{aligned} \quad (\text{E3})$$

and likewise for the identical factor involving n_4, n_5, n_6 . Hence the U^m factorizes into a product of nonlocal operators \hat{b}_R :

$$U^0 \propto \sum_R \hat{b}_R^\dagger \hat{b}_R,$$

where

$$\begin{aligned}
b_R &= \sum_{\sum_i n_i = 3R \bmod N} \left[\sum_{\sum s_i = 0} e^{-\frac{\kappa^2}{2} \sum_i (R - (n_i + N s_i))^2} \right] c_{n_1} c_{n_2} c_{n_3} \\
&= \sum_{n_1 + n_2 + n_3 = 3R \bmod N} \left[\sum_{s,t} e^{-\frac{\kappa^2}{3} W_{st}} \right] c_{n_1} c_{n_2} c_{n_3}, \quad (\text{E4})
\end{aligned}$$

with $W_{st} = \sum_i n_i'^2 - \sum_{i < j} n_i' n_j'$, $n_1' = n_1 + sN$, $n_2' = n_2 + tN$ and $n_3' = n_3 - N(s+t)$. This result is identical to that in Ref. 55.

2. m=1 for bosons on a torus

In this case, the 1st Laguerre polynomial gives a factor $1 - \frac{3}{4}(\kappa^2(n_2 - n_5)^2 + p_x^2)$, and $\sum_{\sigma} P_1$ evaluates to

$$\begin{aligned}
\sum_{\sigma} P_1 &= \sum_{\sigma} 3\kappa^2(n_2 - R)(n_5 - R) \\
&= 3\kappa^2 \left(\frac{n_2 + n_1 + n_3}{3} - R \right) \left(\frac{n_4 + n_5 + n_6}{3} - R \right) \\
&= 0 \quad (\text{E5})
\end{aligned}$$

Hence we have

$$U^1 = 0. \quad (\text{E6})$$

This agrees with the result from Ref. 69, in that there is no PP of total relative angular momentum $m = 1$ for bosons. This is because the CM invariance of the interaction precludes any symmetric wave function of total degree 1.

5. m=4 for bosons on a torus

After the smoke clears, we find

$$U^4 \propto \sum_R \hat{b}_R^\dagger \hat{b}_R,$$

3. m=2 for bosons on a torus

After some algebra,

$$P_2 = \frac{1}{2}(1 - 3\kappa^2(n_2 - R)^2)(1 - 3\kappa^2(n_5 - R)^2).$$

Since

$$\begin{aligned}
\sum_{\sigma} (n_2 - R)^2 &= \sum_{\sigma} (n_2^2 - 2n_2R + R^2) \\
&= \frac{1}{3} \sum_{i=1}^3 n_i^2 - 2R^2 + R^2 \\
&= \frac{2}{9} \left(\sum_i n_i^2 - \sum_{i < j} n_i n_j \right), \quad (\text{E7})
\end{aligned}$$

we have

$$U^2 \propto \sum_R \hat{b}_R^\dagger \hat{b}_R,$$

where

$$\hat{b}_R = \sum_{\sum_i n_i = 3R \bmod N} \left[\sum_{s,t} \left(1 - \frac{2\kappa^2}{3} W_{st} \right) e^{-\frac{\kappa^2}{3} W_{st}} \right] c_{n_1} c_{n_2} c_{n_3} \quad (\text{E8})$$

with $W_{st} = \sum_i n_i'^2 - \sum_{i < j} n_i' n_j'$, $n_1' = n_1 + sN$, $n_2' = n_2 + tN$, and $n_3' = n_3 - N(s+t)$ as before.

4. m=3 for bosons on a torus

This is zero for 2 bosons, but not for 3 bosons⁶⁹. Indeed,

$$\sum_{\sigma} P_3 = \sum_{\sigma} \frac{9}{2} \kappa^6 (n_2 - R)^3 (n_5 - R)^3 = \frac{9}{2} \kappa^6 \prod_{i=1}^6 (n_i - R).$$

Hence

$$U^3 \propto \sum_R \hat{b}_R^\dagger \hat{b}_R,$$

where

$$\hat{b}_R = \frac{-3\kappa^3}{\sqrt{2}} \sum_{n_1 + n_2 + n_3 = 3R \bmod N} \left[\sum_{s,t} (n_1 + sN - R)(n_2 + tN - R)(n_3 - (s+t)N - R) e^{-\frac{\kappa^2}{3} W_{st}} \right] c_{n_1} c_{n_2} c_{n_3}. \quad (\text{E9})$$

where

$$\hat{b}_R = \sum_{\sum_i n_i = 3R \bmod N} \left[\sum_{s,t} \left(1 - \frac{2\kappa^2 W_{st}}{3} + \frac{\kappa^4 W_{st}^2}{9} \right) e^{-\frac{\kappa^2}{3} W_{st}} \right] c_{n_1} c_{n_2} c_{n_3}, \quad (\text{E10})$$

with $W_{st} = \sum_i n'_i{}^2 - \sum_{i<j} n'_i n'_j$, $n'_1 = n_1 + sN$, $n'_2 = n_2 + tN$, and $n'_3 = n_3 - N(s+t)$ as before.

-
- ¹ M. Z. Hasan and C. L. Kane, Rev. Mod. Phys. **82**, 3045 (2010).
- ² X.-L. Qi and S.-C. Zhang, Rev. Mod. Phys. **83**, 1057 (2011).
- ³ J. E. Moore, Nature **464**, 194 (2010).
- ⁴ K. v. Klitzing, G. Dorda, and M. Pepper, Phys. Rev. Lett. **45**, 494 (1980).
- ⁵ D. J. Thouless, M. Kohmoto, M. P. Nightingale, and M. den Nijs, Phys. Rev. Lett. **49**, 405 (1982).
- ⁶ F. D. M. Haldane, Phys. Rev. Lett. **61**, 2015 (1988).
- ⁷ X. L. Qi, Y. S. Wu, and S. C. Zhang, Phys. Rev. B **74**, 085308 (2006).
- ⁸ C.-X. Liu, X.-L. Qi, X. Dai, Z. Fang, and S.-C. Zhang, Phys. Rev. Lett. **101**, 146802 (2008).
- ⁹ R. Yu, W. Zhang, H. J. Zhang, S. C. Zhang, X. Dai, and Z. Fang, Science **329**, 61 (2010).
- ¹⁰ D. C. Tsui, H. L. Stormer, and A. C. Gossard, Phys. Rev. Lett. **48**, 1559 (1982).
- ¹¹ R. B. Laughlin, Phys. Rev. Lett. **50**, 1395 (1983).
- ¹² X. G. Wen, Phys. Rev. B **40**, 7387 (1989).
- ¹³ G. Moore and N. Read, Nucl. Phys. B **360**, 362 (1991).
- ¹⁴ C. Nayak, S. H. Simon, A. Stern, M. Freedman, and S. Das Sarma, Rev. Mod. Phys. **80**, 1083 (2008).
- ¹⁵ E. Tang, J.-W. Mei, and X.-G. Wen, Phys. Rev. Lett. **106**, 236802 (2011).
- ¹⁶ T. Neupert, L. Santos, C. Chamon, and C. Mudry, Phys. Rev. Lett. **106**, 236804 (2011).
- ¹⁷ K. Sun, Z. Gu, H. Katsura, and S. Das Sarma, Phys. Rev. Lett. **106**, 236803 (2011).
- ¹⁸ J. W. F. Venderbos, M. Daghofer, and J. van den Brink, Phys. Rev. Lett. **107**, 116401 (2011).
- ¹⁹ D. Xiao, W. Zhu, R. Y., N. Nagaosa, and S. Okamoto, Nature Comm. **2**, 596 (2011).
- ²⁰ D. N. Sheng, Z.-C. Gu, K. Sun, and L. Sheng, Nature Comm. **2**, 389 (2011).
- ²¹ N. Regnault and B. A. Bernevig, Phys. Rev. X **1**, 021014 (2011).
- ²² S. M. Girvin, A. H. MacDonald, and P. M. Platzman, Phys. Rev. B **33**, 2481 (1986).
- ²³ S. A. Parameswaran, R. Roy, and S. L. Sondhi, Phys. Rev. B **85**, 241308 (2012).
- ²⁴ G. Murthy and R. Shankar, arXiv:1207.2133.
- ²⁵ X.-L. Qi, Phys. Rev. Lett. **107**, 126803 (2011).
- ²⁶ Y.-L. Wu, N. Regnault, and B. A. Bernevig, Phys. Rev. B **86**, 085129 (2012).
- ²⁷ T. Scaffidi and G. Möller, Phys. Rev. Lett. **109**, 246805 (2012).
- ²⁸ F. D. M. Haldane, Phys. Rev. Lett. **51**, 605 (1983).
- ²⁹ F. D. M. Haldane and E. H. Rezayi, Phys. Rev. B **31**, 2529 (1985).
- ³⁰ S. H. Simon, E. H. Rezayi, and N. R. Cooper, Phys. Rev. B **75**, 075318 (2007).
- ³¹ R. Thomale, B. A. Bernevig, and M. Greiter, in preparation.
- ³² F. D. M. Haldane, Phys. Rev. Lett. **55**, 2095 (1985).
- ³³ B. A. Bernevig and N. Regnault, Phys. Rev. B **85**, 075128 (2012).
- ³⁴ R. Yu, X.-L. Qi, B. A. Bernevig, Z. Fang, and X. Dai, Phys. Rev. B **84**, 075119 (2011).
- ³⁵ S. Kivelson, Phys. Rev. B **26**, 4269 (1982).
- ³⁶ R. D. King-Smith and D. Vanderbilt, Phys. Rev. B **47**, 1651 (1993).
- ³⁷ M. Abramowitz and I. Stegun, *Handbook of Mathematical Functions* (Dover, New York, 1965).
- ³⁸ D.-H. Lee and J. M. Leinaas, Phys. Rev. Lett. **92**, 096401 (2004).
- ³⁹ M. Barkeshli and X.-L. Qi, Phys. Rev. X **2**, 031013 (2012).
- ⁴⁰ G. Fano, F. Ortolani, and E. Colombo, Phys. Rev. B **34**, 2670 (1986).
- ⁴¹ N. Read and E. Rezayi, Phys. Rev. B **59**, 8084 (1999).
- ⁴² E. H. Rezayi and F. D. M. Haldane, Phys. Rev. B **50**, 17199 (1994).
- ⁴³ A. Seidel, H. Fu, D.-H. Lee, J. M. Leinaas, and J. Moore, Phys. Rev. Lett. **95**, 266405 (2005).
- ⁴⁴ S. A. Trugman and S. Kivelson, Phys. Rev. B **31**, 5280 (1985).
- ⁴⁵ X. G. Wen and Q. Niu, Phys. Rev. B **41**, 9377 (1990).
- ⁴⁶ E. J. Bergholtz and A. Karlhede, Phys. Rev. B **77**, 155308 (2008).
- ⁴⁷ Y.-F. Wang, Z.-C. Gu, C.-D. Gong, and D. Sheng, Phys. Rev. Lett. **107**, 146803 (2011).
- ⁴⁸ the original CB model¹⁷ distinguishes between two types of NNN hoppings t'_1 and t'_2 , but the constraint $t' = t'_1 = -t'_2$ is sufficient to produce a band of maximum flatness.
- ⁴⁹ H. Li and F. D. M. Haldane, Phys. Rev. Lett. **101**, 010504 (2008).
- ⁵⁰ R. Thomale, A. Sterdyniak, N. Regnault, and B. A. Bernevig, Phys. Rev. Lett. **104**, 180502 (2010).
- ⁵¹ T. Liu, C. Repellin, B. A. Bernevig, and N. Regnault, Phys. Rev. B **87**, 205136 (2013).
- ⁵² A. G. Grushin, T. Neupert, C. Chamon, and C. Mudry, Phys. Rev. B **86**, 205125 (2012).
- ⁵³ M. Greiter, X. G. Wen, and F. Wilczek, Phys. Rev. Lett. **66**, 3205 (1991).
- ⁵⁴ S. H. Simon, E. H. Rezayi, and N. R. Cooper, Phys. Rev. B **75**, 195306 (2007).
- ⁵⁵ A. Seidel and D. Lee, Phys. Rev. Lett. **97**, 056804 (2006).
- ⁵⁶ D. Yoshioka, A. H. MacDonald, and S. M. Girvin, Phys. Rev. B **38**, 3636 (1988).
- ⁵⁷ M. Greiter, Bull. Am. Phys. Soc. **38**, 137 (1993).
- ⁵⁸ S. H. Simon, E. H. Rezayi, N. R. Cooper, and I. Berdnikov, Phys. Rev. B **75**, 075317 (2007).
- ⁵⁹ C.-H. Chern, Phys. Rev. B **81**, 115123 (2010).
- ⁶⁰ F. Wang and Y. Ran, Phys. Rev. B **84**, 241103 (2011).
- ⁶¹ M. Trescher and E. J. Bergholtz, Phys. Rev. B **86**, 241111(R) (2012).
- ⁶² S. Yang, Z.-C. Gu, K. Sun, and S. Das Sarma, Phys. Rev. B **86**, 241112(R) (2012).
- ⁶³ Z. Liu, E. J. Bergholtz, H. Fan, and A. M. Läuchli, Phys. Rev. Lett. **109**, 186805 (2012).
- ⁶⁴ M. Levin and A. Stern, Phys. Rev. Lett. **103**, 196803 (2009).
- ⁶⁵ B. Scharfenberger, R. Thomale, and M. Greiter, Phys. Rev. B **84**, 140404 (2011).

- ⁶⁶ T. Neupert, L. Santos, S. Ryu, C. Chamon, and C. Mudry, Phys. Rev. B **84**, 165107 (2011).
- ⁶⁷ Y.-M. Lu and Y. Ran, Phys. Rev. B **85**, 165134 (2012).
- ⁶⁸ J. Jain, *Composite Fermions* (Cambridge University Press, London, 2007).
- ⁶⁹ S. Simon, E. Rezayi, and N. Cooper, Phys. Rev. B **75**, 195306 (2007).
- ⁷⁰ Y.-F. Wang, H. Yao, Z.-C. Gu, C.-D. Gong, D.N. Sheng, Phys. Rev. Lett. **108**, 126805 (2012).